AN INVESTIGATION INTO THIN FILM PALLADIUM ALLOY COMPOSITE MEMBRANES WITH A POWDERED TUNGSTEN INTERMEDIATE LAYER FOR THE SEPARATION OF HYDROGEN

by

GEORGE INNES SIMPSON

A thesis submitted to

The University of Birmingham

For the degree of

MASTER OF RESEARCH

School of Metallurgy and Materials

College of Engineering and Physical Sciences

The University of Birmingham

July 2011

Synopsis

The development of a composite (Pd-alloy thin film / Porous stainless steel substrate) hydrogen separation membrane was investigated, that can operate at high temperatures (600°C), for use in a hydrocarbon reformation reactor for the production of pure hydrogen.

An intermediated layer of tungsten powder with a particle size of >1 μm was deposited onto the surface of macroporous 316L stainless steel (PSS) substrates. This layer served to: create an interdiffusion barrier against iron diffusion from the PSS into the Pd-alloy thin film (and so preventing the formation of Pd-Fe phases with low hydrogen permeability); and also to reduce the surface pore size of the PSS, to aid the thin-film sputtering process. The dual performance of this intermediate layer within a composite membrane was tested, in terms of surface pore size reduction and ability to prevent interdiffusion.

The extent of the powder filling and surface pore reduction was calculated along with the effect on hydrogen transport through the modified substrate. The results showed that both one and three layers of tungsten powder were successful. One tungsten layer reduced surface pore size by an average percentage difference of 50% (from 8 to 4 μm), and also did not significantly inhibit hydrogen flux through the substrate, with a range of hydrogen flux decrease values from 8- 25%.

Production of a defect-free membrane layer was also investigated, coating the tungsten modified PSS substrate with various thicknesses of stainless steel (SS) (as a low-cost proxy for a Pd-alloy thin film). The results showed that a more continuous defect-free membrane layer was achieved when the surface of the substrate was most uniform. In successful samples, where the tungsten coating was seeming filling the pores more accurately there was

up to a 72% reduction in surface pore size. This only required 20 μm of SS to give a 94% reduction in hydrogen flux.

The performance of both dense and powdered tungsten intermediate barriers on their ability to prevent iron diffusing into sputtered Pd/PdCu membrane layers, was also investigated. Samples were heated to 600°C in a helium atmosphere. SEM-EDX analysis showed that dense tungsten was very successful at preventing iron diffusion while the powdered particles were also clearly preventing interdiffusion within the pores.

It is concluded that a combination of both dense and powdered tungsten would need to be used to fully prevent iron diffusion. In terms of surface pore filling, a refinement of the deposition technique used to deposit the tungsten powder would need to be developed in order to produce a more even surface profile and therefore result in a more continuous defect-free membrane layer.

Acknowledgments

I would like to express my genuine thanks to Dr. David Book and especially Dr. Sean Fletcher for their help, advice and support during the supervision of this project.

Table of Contents

Chapter 1- Introduction

Section 1- Introduction

Hydrogen energy has caught the attention of the energy industry due to its potential as an energy vector, which may contribute towards alleviating environmental concerns and strengthening energy security. Research and development into hydrogen production and utilization have been conducted by many researchers, across the globe. Hydrogen has been utilized in a number of industries including: hydro-desulphurisation and hydro-cracking within the petrochemical industry; as a reducing agent for metals in Fischer-Tropsch reactions [1], ammonia production for fertilisers [2], and as a carrier gas for the doping of silicon wafers in the semi-conductor industry [3].

Fuel cells are expected to be the major technology for hydrogen utilization, with the proton exchange membrane (PEM) fuel cell being the most widely used as a power unit for vehicles, residential co-generation, and a power unit for mobile energy generation; such as membrane reactors. Current global unease over climate change is likely to increase the demand for an alternative clean energy source. As PEM fuel cells only produce H_2O as a by-product they are an attractive prospect.

However, for a PEM fuel cell to be operational it needs a source of ultra high purity hydrogen. Molecular hydrogen can be produced via the electrolysis of water or more commonly it is

produced by the steam reformation reaction (SMR). [4] This involves a two stage process that is carried out at 800°C, and can be summarised by Equation 1.1.[5]

$$CH_4 + 2H_2O \Leftrightarrow CO_2 + 4H_2$$

$\Delta H = +206$ kJ/mol ***Equation 1.1***

The product gas stream after steam reforming is typically 74 % H_2, 18 % CO_2, 7 % CH_4 and 1 % CO [5], which is not pure enough to be used in a PEM fuel cell or for materials processing in the electronics industry. Therefore, a second purification stage is needed to reach the necessary 99.99999 % purity level [6]. Usually dense metal membranes are used and offer a convenient separation method as a standalone device. Dense membranes can also be used in combination with the SMR process inside a unit known as a membrane reactor. This combines the reforming process with the dense metal membrane's ability to further purify the gas in single portable application.

Hydrogen production technologies using fossil fuels such as natural gas and coal are not clean energy sources when compared to those from wind or solar, emitting large quantities of green house gases during their lifetime [4]. However, the technology has been used in the oil refining industry for decades and is well-established and is economical. In order for the hydrogen economy to grow, SMR must be used as a bridging technology in order to produce the large volumes of hydrogen that will be required.

The membrane reactor system is compact, simpler, and more efficient than the two-stage process of conventional steam methane reforming (SMR). The dense metal membranes used at present within the system are self-supporting rolled foils or drawn tubes, with a typical thickness of ~ 50 μm. The hydrogen flux through this relatively thick membrane is much lower than the targets expressed by the US department of energy (DoE) [7]. As hydrogen flux is directly proportional to membrane film thickness, reducing the film to (< 5 μm) has the potential to meet these targets and also reduce the amount of Palladium (Pd) used.

Using such thin films requires a number of considerations and there is not yet an easy solution. Thin films with thicknesses below 50 μm do no longer have the structural integrity to resist the thermal and mechanical stresses experienced during operation and therefore require a mechanical support. A number of supports have been suggested, with ceramic [8] and porous stainless steel (PSS) [9] being amongst the most popular. Each one has their advantages and disadvantages, with porous stainless steel offering the most compatible characteristics. Coating a thin metallic membrane layer, such as Pd onto the surface of a mechanical support is not a straightforward process, and considerable work is needed to modify the surface pore size in order to produce a continuous defect-free layer. Temperatures within a membrane reactor can reach 600°C and therefore intermetallic diffusion is a problem that causes hydrogen flux to rapidly decrease, therefore membranes require an interdiffusion barrier to combat this problem.

A number of interdiffusion barriers have been investigated, including: Yttria-stabilised Zirconia [10], Oxides [11], and Tungsten [12]. Each are successful at preventing interdiffusion;

however simply preventing the flow of Fe ions does not address the other pressing issue of pore size reduction. For thin film membranes to be successful in the future, both issues must be dealt with, as one without the other will not meet the DoE targets.

Chapter 2- Literature review

Section 2- Hydrogen separation

2.1- Introduction

At present, manufacturers typically produce ultra-pure hydrogen by a costly two-stage process. A mixture of 74 % H_2, 18 % CO_2, 7 % CH_4 and 1 % CO is produced by the reformation of steam [5], which can then be purified using a system based on a dense Pd-Ag membrane. This system falls short of the desired performances targets set out by the US Department of energy as it is costly and slow. The current focus is to combine the two processes in a scaled down system called a membrane reactor that can be used as a standalone unit. An example of a membrane reactor is shown in Figure 1, where the palladium-based membrane is incorporated within the reformation reaction.

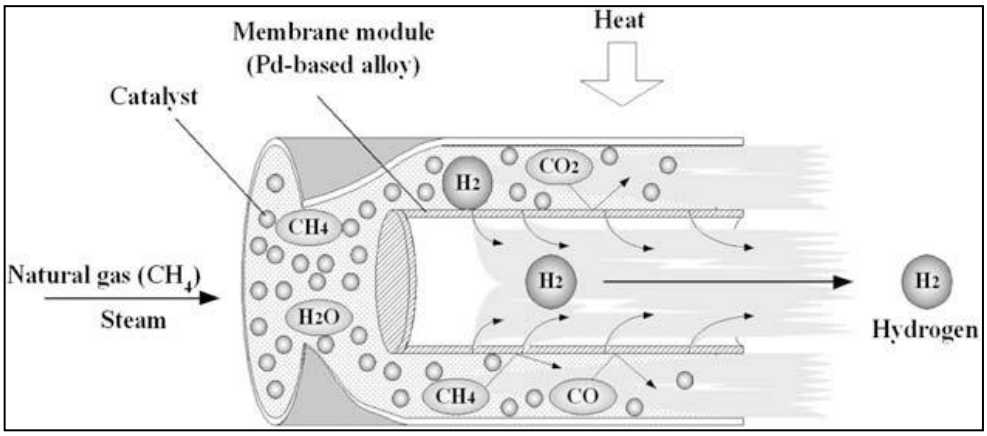

Figure 1- Membrane reactor in operation taken from Shirasaki, Y., et al. [13]

Combining palladium membranes within a membrane reactor poses a number of issues. The membrane would be subjected to constant high temperature conditions and would need to

withstand the impurities of a mixed gas stream. The standalone unit also seeks to increase the kinetics at which the hydrogen is dissociated, using less expensive palladium. Therefore, there has been increased interest in research into thin-film membranes, which have the potential to fulfil these challenging requirements. However, utilising thin and fragile materials possess a number of metallurgical problems, including the type of porous support material and the interaction between them both at particular temperatures.

2.2 Hydrogen Production

2.2.1 Steam reformation

Steam reformation of natural gas is currently the least expensive method and is responsible for more than 90 % of hydrogen production worldwide [4]. Natural gas is firstly cleared of sulphur compounds, and then it is combined with steam over a nickel-alumina catalyst inside a tubular reactor. This reactor is heated externally to above 800°C [5] and is where carbon monoxide (CO) and hydrogen (H_2) are generated.

$$CH_4 + H_2O <=> CO + 3\ H_2$$

$\Delta H = +206kJ/mol$ ***Equation 2.1***

This step is followed by a catalytic water-gas shift reaction, which converts the CO and water to hydrogen and carbon dioxide (CO_2), see *Eq 2.2*.

$$CO + H_2O <=> CO_2 + H_2$$

$\Delta H = -41kJ/mol$ ***Equation 2.2***

The overall reaction can be summarised as:

$$CH_4 + 2H_2O <=> CO_2 + 4H_2$$

$\Delta H = +165kJ/mol$ ***Equation 2.3***

The technology is suitable for large reformers (e.g. 100 000 tons of H_2 per year) [14], where yields higher than 80 % can be achieved. However, this process does not give the high purity needed for PEM fuel cell applications and in the electronics industry, so therefore a further separation stage is required.

2.2.2 Pressure Swing Adsorption

The pressure swing adsorption (PSA) process utilises certain materials ability to readily adsorb impurity molecules from a mixed gas stream at high partial pressures, and to then subsequently desorb the impurities at low partial pressures.

Typically a mixed gas stream would flow through a chamber containing an adsorbent such as a zeolite which has a very high surface area. At relatively high pressures (1500-2000 kPa) the impurities are adsorbed onto the adsorbent surface while the hydrogen permeates through. Once the adsorbent has reached saturation the impurity partial pressure is decreased by 'swinging' the system pressure from the feed gas pressure to the pure hydrogen permeate pressure. A purge gas at a low pressure is applied to the system and the impurities subsequently desorb and are removed from the system.

The benefits of using PSA are its ability to produce a range of purities with a relatively high maximum purity of 99.999 % and the systems durability is also an advantage with adsorbents

lasting the life time of the equipment [15]. Despite these advantages, PSA is medium-high level production method requiring expensive running and equipment costs which makes it unsuitable for portable applications such as membrane reactors.

2.2.3 Hydrogen selective membranes

Currently, hydrogen selective membranes are used to separate very low volumes of hydrogen for the semiconductor and LED industries. Dense metal membranes, usually made from a palladium alloy are used to separate the hydrogen, and give very high purity outputs. Pd alloys such as Pd-Ag are commercially used instead of pure Pd because of the exhibited miscibility gap, which causes failure at temperatures up to 300°C: this is explained in more depth in Section 3.3. This simple procedure relies on a concentration gradient being applied across a sealed semi-permeable barrier. Hydrogen will then only permeate across the dense metal membrane and other gasses with be rejected. This permeation takes place via a solution-diffusion mechanism which can be considered in a seven stage process [16].

1. Molecular transport from the bulk gas to the gas layer adjacent to the surface
2. Dissociative adsorption of molecular hydrogen onto the high-pressure surface where atomic H is held at active surface sites.
3. Transition of atomic H from the surface into the bulk metal.
4. Atomic diffusion of H through the metal lattice to a point just inside the low-pressure surface.
5. Transition from the bulk metal to active surface sites on the low pressure surface
6. Recombinative desorption on the surface
7. Gas transport away from the surface into the bulk gas.

Each one of the steps has a relative contribution at given operating conditions; therefore the rate at which hydrogen is permeated through the membrane can be limited via just one of the seven steps. For example, group 5 transition metals such as V and Nb both theoretically have very high permeabilities; however their overall affinity for hydrogen permeation is hampered by their thick surface oxide layers, which limit the absorption and desorption of hydrogen onto the surface [17].

Palladium is one of the most effective materials for hydrogen separation as it has high affinity for hydrogen dissociation. Only diffusion of molecules through the lattice is a limiting factor. Therefore, in order to increase performance of the membrane either the permeability needs to improve, or the thickness of the membrane needs to significantly decrease.

Equation 2.4, where J_{H_2} is the hydrogen flux ($mol.m^{-2}.s^{-1}$) is directly proportional to both permeability ($mol.m^{-1}.s^{-1}.Ps^{-0.5}$) (ø) and the partial pressure gradient (Pi-Pii). The thickness (L) is shown to be inversely proportional to the flow rate J_H. Reducing the thickness of the membrane not only increases the flux, it also reduces the material cost of the membrane, as Pd is an expensive commodity.

$$J_{H_2} = ø\ Pi - Pii / L$$

Equation 2.4

Commercially available membranes have a typical thickness of around 50 μm which enables the membranes to be self-supporting but at the same time give the best possible flux rates. These membranes are generally manufactured using techniques such as cold rolling and drawing. In this case, with thickness being set at 50 μm, attention turned to increasing the permeability of the material. A number of studies were carried out on binary and ternary

alloys [18] of Pd in an attempt to further increase the permeability (and lower the cost) compared to Pd alone. Commercially available membranes such as Pd-Ag are shown to have 3x the permeability of pure Pd, while other alloys such as Pd-Cu and Pd-Y have shown to increase permeability by a significant amount. At 300^{o}C an addition of just 1.68 at% Y increases permeability by 80% compared to pure Pd, whilst adding ~8at.% Y increases permeability by over a factor of 5. At 350°C the permeability of hydrogen in Pd-Y_8 is found to be 5.92 x10^{-8} mol.m^{-1}.s^{-1}.$Pa^{-0.5}$ [19].

The US Department of Energy (DoE) has suggested a number of targets that need to be reached, in the hydrogen production technology industry.[7]

Table 1- US Department of Energy target data [7]

Performance Criteria	**Units**	**2010 target**	**2015 target**
H_2 flux [400°C]	Mol.m^{-2}.s^{-1}	0.945	1.134
Cost	\$US.ft^{-2}	1000	<500
Durability	Hr	26,280	43,800
Operating Pressure	Psi (Bar)	400 (27.58)	400-600 (27.58-41.37)

The targets outlined are based on the anticipated levels for the technology to be economically competitive with the current hydro-carbon based technologies. Therefore, in order to reach these targets, research must not only look at increasing the permeability of the membrane, but to also examine ways of decreasing the thickness in order to increase the rate of hydrogen permeation (flux).

Section 3-Thin film palladium and palladium-alloy membranes

3.1 Introduction

Thin film membranes are usually less than 20 µm in thickness and are therefore unable to be free standing unlike dense film membranes. For a thin film (<10 µm) to be functional it needs to be deposited onto an underlying structure. The substrate has to be able to support the film and maintain its structural integrity throughout the chosen operating conditions. Thin film membranes with a thickness less than 10 µm, are limited in that they do not have the mechanical strength to withstand the stresses of thermal expansion, lattice expansion with H adsorption, and pressure gradients across the membrane associated with operation. Therefore, it is essential that they are used in conjunction with a mechanical support. The dense thin film still acts as a selective diffusion barrier, and for ultra high purity hydrogen this layer needs to be completely continuous with no defects. The support material needs to be highly porous, offering minimal gas flow resistance, whilst maintaining its structural integrity. This multi-layered construction, as shown in Figure 2, is often referred to as a composite membrane.

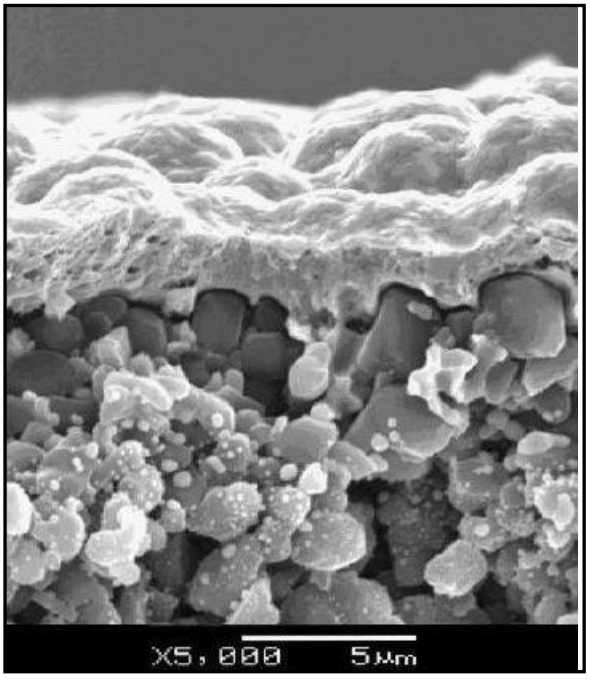

Figure 2- A Pd-Ag5 / α-alumina thin film composite membrane. Taken from Zeng et al [20]

3.2 Membrane integrity and defects

The quality of the Pd alloy film coated onto the porous substrate is evaluated in terms of its selectivity, which is defined as the H_2 / N_2 flux ratio across the membrane. A defect-free membrane with a continuous layer of Pd alloy would demonstrate infinite selectivity, as only hydrogen would be able to permeate across the dense layer.

The main performance barrier of the Pd alloy layer is the deposition of a non-continuous layer or the development of pinholes. The term 'pinhole' is broadly used to describe any sort of surface defect, including both microscopic and macroscopic. Microscopic defects are normally breaks in the film along grain boundaries or are due to voids within the crystal structure. Macroscopic defects can include open pores due simply to poor coverage, and splits/ cracks due to localised areas of delamination during thermal cycling or to the lattice expansion experienced during hydrogen adsorption (Figure 3). Macroscopic defects have been

shown to have the greatest effect on hydrogen selection and a number of studies have looked at various fabrication methods in order to eliminate such pinholes.

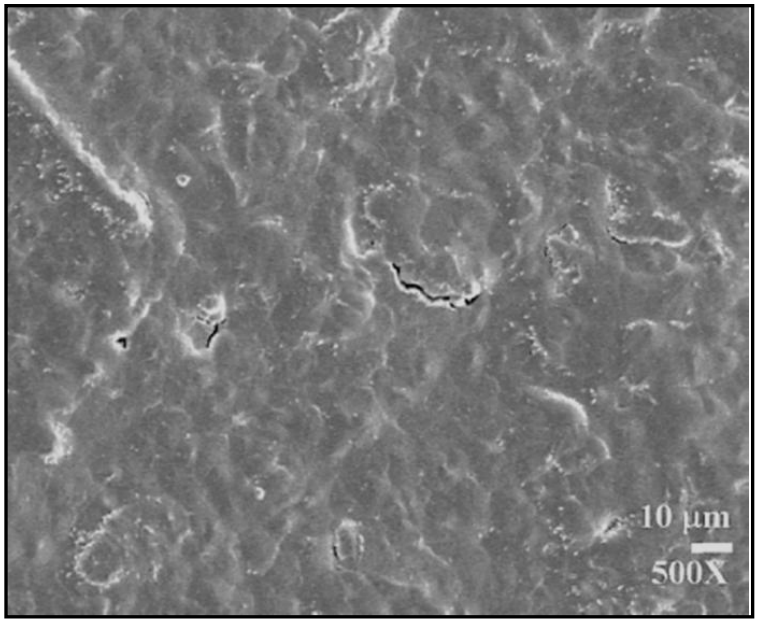

Figure 3- SEM secondary electron image of an example of macroscopic defects in a sputtered 5µm Pd membrane. Taken from Checchetto et al [21]

In order to guarantee a continuous defect-free layer, the substrate surface must first be completely clean and free of debris. Once this is achieved the predominant factors that affect surface coverage are pore size, surface roughness and film thickness [22] [23] [24, 25]. The general consensus in the literature is that membrane thickness generally decreases with surface pore size, although there have been a number of studies that suggest that there is a limit, beneath which the surface becomes too smooth [26] [27]. A membrane needs a certain amount of surface roughness in order to mechanically adhere itself to the underlying substrate; a surface with extremely small pores will therefore suffer from poor adhesion and ultimately delamination. Roa et al [26] found that when depositing membranes onto γ-alumina substrates with an average pore size of 5 nm, they were unable to produce a continuous defect-free layer.

However, they did find that substrates with a larger pore size of 50 nm and 200 nm were able to be coated with a highly selective layer. Ma et al [28] suggested that in order to deposit a continuous defect-free layer, thickness must be 3 times the maximum pore size of the substrate.

3.3 Pd and Pd-alloy thin films

Dense palladium (Pd) thin-film membranes are capable of adsorbing large volumes of hydrogen whilst still retaining their physical properties and structural integrity [29]. Dense palladium also possesses superior hydrogen selectivity and fast diffusion rates when compared to other refractory metals with the body centred cubic (BCC) crystal structure such as vanadium and niobium, which have very inactive surfaces for the dissociation of molecular hydrogen and thus have slow surface adsorption and desorption rates [17].

However, pure Pd is not suitable for membrane operation. When a pure Pd membrane is exposed to a mixed feed gas with contaminants – such as, sulphur species, carbon monoxide, carbon dioxide and water vapour – they poison the Pd membrane, resulting in a significant decreased in separation performance. The main problem however, is due to the Pd-H system exhibiting two immiscible fcc phases: α (interstitial solid solution), and β (palladium hydride). Failure of the membrane is seen when there is a transition from α to β which causes volume expansion of the lattice [30]. This transition causes stresses within the structure, which causes embrittlement and ultimately failure. At temperatures above 293°C the miscibility gap (the difference between α and β phases) is eliminated as only the α solid solution phase is maintained [31]. Therefore pure palladium membranes are limited to use above this temperature.

Pd has been alloyed with a number of different elements such as Ag [32], Ni [33], Cu [34], Ru [12]. In the case of PdCu and PdAu (Figure 4), alloying not only reduces poisoning but also

suppresses the miscibility gap to below room temperature thereby making operating conditions much more desirable. However, many researchers still use pure palladium as their dense selective layer, because they are restricted to using electroless plating as their method of coating. Electroless plating is one of two main methods used, and has the advantage of being a very easy technique with the ability to deposit a wide range of membrane thicknesses. However, electroless plated films regularly possess significantly lower densities than the comparable bulk material, caused by voids and impurities such as carbon or tin. Indeed, carbon contents of up 6.5 wt.% have been reported within electrolessly deposited Pd membranes [35]

One of the most successful alloys is PdAu, which has been used commercially to a great extent; however the alloy combination of palladium and copper has also to be successful. Alloying palladium with copper (Cu_{40}wt %) enables the membrane to have a similar permeability to that of pure Pd, whilst having the added resistance to hydrogen embrittlement and poisoning by gaseous impurities such as CO and H_2S [36], and the advantage of lower material costs.

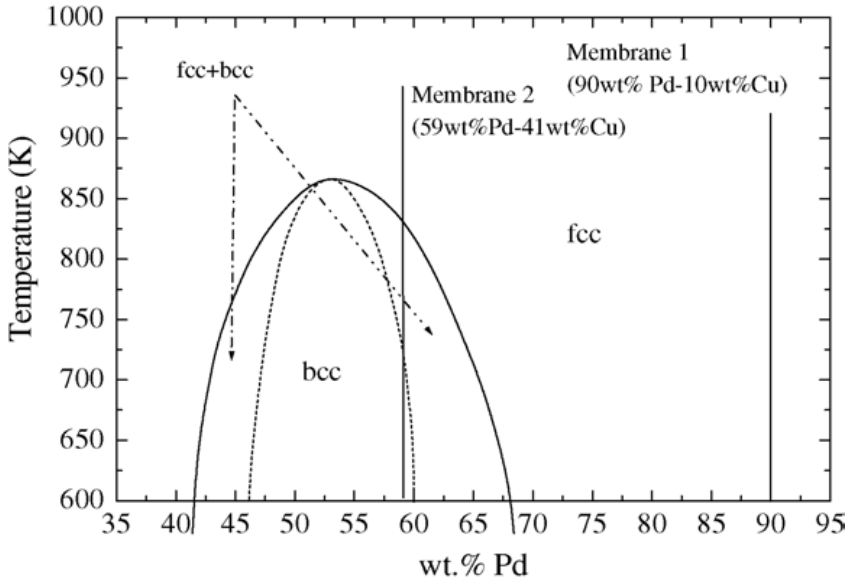

Figure 4- Binary Phase diagram of PdCu [36]

Section 4- Deposition techniques

When a thin film is deposited onto a porous substrate it is generally referred to as a composite membrane. The most typical type of composite membrane is either a porous stainless steel or porous ceramic substrate coated with pure or alloyed palladium. There are numerous ways of depositing dense thin films, including: chemical vapour deposition, electrodeposition, electroless plating, and physical vapour deposition (PVD). The two most common used are, electroless plating and magnetron sputtering.

Magnetron sputtering is a widely used deposition technique, where single-phase solid solution alloys can be deposited without the need for thermal homogenisation [22]. The sputtering process involves gas plasma bombarding a metal target, whereby metal atoms are subsequently dislodged and deposited onto the substrate. Yang [37] demonstrated that film thickness is directly proportional to sputtering time shown in figure 5, therefore allowing accurate control of film thickness. A number of Pd-Ag [38] and Pd-Cu [37, 39] membranes have been deposited from single metal targets with success.

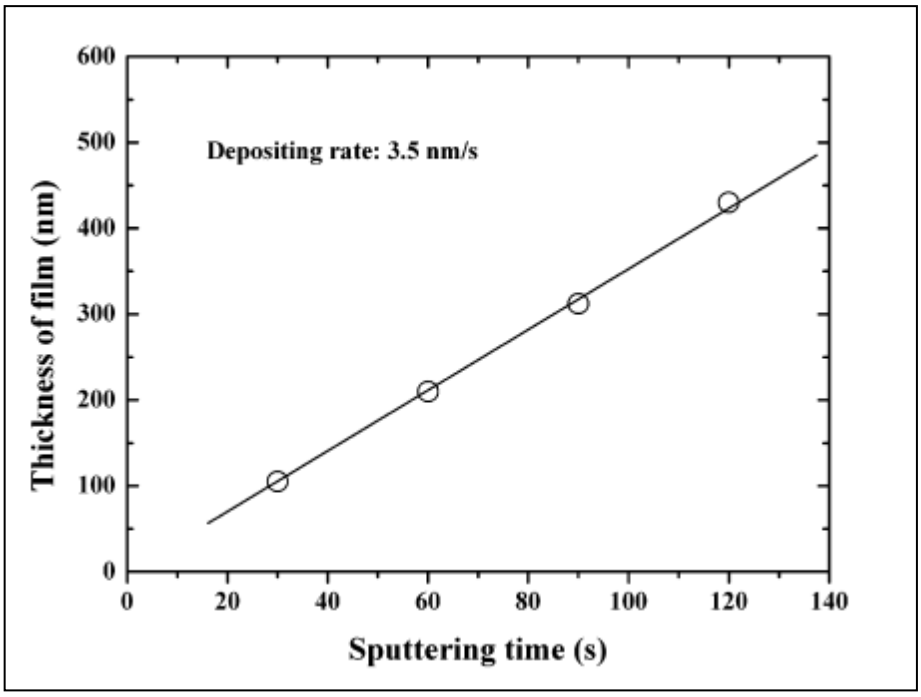

Figure 5- Variation of Pd_{60}-Cu_{40} thickness with sputtering time. [37]

Another advantage of the sputtering technique is that prior to film deposition, the gas plasma can be applied to the sample substrates in order to clean the surface. This is a very important feature as the cleanliness of the coating surface is paramount to producing a membrane with a defect-free layer.

Yang et al [37] used magnetron sputtering to produce a PdCu alloy. Positioning the two desired targets next to each other in the vacuum chamber and employing rotation of the samples enables the coating of a single solid solution alloy. Yang et al [37] showed that they were not only able to get excellent thickness and compositional reproducibility when depositing PdCu, they were also able to produce homogenous solid solution alloys without the need for post-deposition thermal treatment.

Although magnetron sputtering seems to fulfil many of the desired requirements it is not widely available due to equipment costs [40]. The other more widely available and simple option utilised by many research groups is electroless plating. This technique involves three

stages: surface cleaning, surface activation, and film deposition. The cleaning stage involves washing firstly in dilute acid, alcohol or acetone, and then rinsing in de-ionised water. Tin chloride and palladium activation baths are then used to activate the surface of the sample, and then via the chemical reduction of Pd ions the sample can be coated. This process is repeated until the desired coating thickness is achieved, [41] [42]. Although a relatively simple process, electroless plating has a few important drawbacks. Producing solid solution alloys via this method has proved difficult [43]; groups have deposited pure element layers, e.g. Pd, Ag, Pd, Ag and then annealed them to form an alloy [44], however this method is time-intensive and dependant on a number of variables. Reproducing desired thicknesses and compositions can also be difficult.

Section 5- Porous supports

5.1 Types of porous support

There are several different materials used to support thin film Pd or Pd-alloy membranes, including: titania [45]; porous ceramics, such as alumina [42]; zirconia [36]; porous glass [46]; nickel [47]; and porous metals, such as stainless steel [48]. The most common supports are ceramic and porous stainless steel (PSS). The main advantages to using ceramic substrates are their fine pore size, and their ability to maintain chemical stability at elevated temperatures. The ability to use the membranes at elevated temperatures, in some cases reaching in excess of 800°C [49] would theoretically enable the use inside a membrane reactor.

Fine pore sizes exhibited by ceramics allows for a reduced thickness in Pd alloy layer without compromising the membrane purification performance as a more continuous layer is less likely develop pinholes. However, the main drawback to using ceramics is that they have a dissimilar thermal expansion co-efficient to that of Pd. This difference leads to stresses

forming within the film and at the interface, which causes the film to delaminate and ultimately fail. Keuler [32] coated a 2 μm thick Pd-Ag layer via electroless deposition onto an alumina substrate. They found that the selectivity of the membrane was good at low temperatures, showing a small density of pinholes, but as the temperature increased to 550°C, selectivity was reduced indicating defect formation and film delamination. Therefore, in order for the films to be successfully used inside a membrane reactor, which reaches temperatures above 600°C, the thermal expansion issue must be resolved.

Sintered metal powders such as porous stainless steel (PSS) are also widely used, due to their similar thermal expansion co-efficient, joinability /solderability, low cost, and good adhesion qualities when compared to a ceramic substrate. Porous metallic substrates generally have a relatively large pore size 10-30 μm, which makes coating continuous thin (< 5 μm) Pd layers difficult. The minimum thickness required to form a dense layer is heavily dependent on the underlying surface on which it is coated. The larger the pore size of the substrate surface, the thicker the layer has to be in order to produce a continuous layer. Ma et al [28] suggested that in order to deposit a continuous defect-free layer, it must be 3 times the maximum pore size of the substrate.

Researchers have tried a number of ways to modify the surface, including Ryi et al [47] who attempted using a porous nickel substrate with much finer surface pores. This did in fact enable a thin Pd layer to be coated but the low porosity significantly hindered hydrogen flux. It is clear, therefore, that although it is desirable to minimise pore size in order to facilitate the deposition of a dense Pd-based layer, there is a limit beyond which further reductions in pore size will offer increased resistance to hydrogen flow and the membrane layer will no long be the rate limiting factor.

Although porous stainless steel offers a number of advantages over ceramic substrates, another issue of concern is the inter-diffusion experienced at the interface between the substrate and Pd-based membrane layer. At high temperatures of 600°C, such as in a membrane reactor, inter-metallic diffusion will take place, which reduces H_2 solubility and greatly reduces the diffusion coefficient in the Pd layer, ultimately resulting in a decline in performance. Diffusion of Fe into the Pd layer is the most common problem for PSS/Pd systems. Bryden & Ying [50] found that the hydrogen permeability of Pd-$Fe_{2.5at\%}$ was over 50 % lower than pure Pd. The formation of Pd_3Fe, which has a larger lattice, causes lattice expansion which greatly reduces performance by increasing the amount of defects within the lattice. In order to combat this problem a number of interdiffusion barriers have been suggested (Chap 2 Section 7), which all aim to prevent the flow of Fe into the palladium lattice.

Section 6- Hydrogen permeation

6.1 PSS substrate

In order to understand the diffusion path, the shape and pore size of the substrate discs needs to be defined. The two important geometries that therefore need to be calculated are the porosity (ε), which is characterised by the amount of open space within the structure and the tortuosity (τ), which considers the tortuous nature of the structure. Equation 6.1 defines the flux due to Knudsen diffusion where l is the substrate thickness, M the molecular mass, R the gas constant, T the absolute temperature and P is the pressure.

$$J_K = \frac{2}{3}\frac{\varepsilon r}{\tau}\frac{1}{l}\left(\frac{8}{\pi\, R\, T\, M}\right)\Delta P$$

Equation 6.1

It is apparent form this equation that flux due to Knudsen flow is proportional to the average pore radius *r* and also the square root of the molecular mass *M*. If the Knudsen number $K_{n,}$ which is defined as the ratio between the number of molecule-molecule collisions to that of the molecule-wall collisions is much smaller than unity (<<1), the number of intermolecular collisions are strongly dominant and the gas flow is said to be dominated by laminar Poiseuille flow. Considering this the hydrogen flux can be shown using the Hagan-Poiseuille law in Equation 6.2. [51]

$$J_V = -\frac{r^2}{8\eta}\frac{P_T}{RT}\frac{\Delta P}{\Delta x}$$

Equation 6.2

Where η denotes the viscosity, P_T the total pressure, r^2 the pore radius. The equation needs to be adapted to take into account the geometric factors considered in the previous equation. $P\frac{\Delta P}{\Delta x}$ can be assumed constant under steady state conditions due to the flux in and out of the pores being equal. The flux is therefore given as,

$$J_v = \frac{1}{8}\frac{\varepsilon}{\tau\eta}\frac{r^2}{R\ T\ l}P_{av}\,\Delta P$$

Equation 6.3

Where P_{av} is the average pressure across the substrate. It is clear to see form the equation that Poiseuille flow is proportional to both the mean pore radius squared r^2, average pressure across the substrate P_{av} , and viscosity.

Generally for pores with a average radius of >1.5 nm there is a combined effect of both Poiseuille flow and Knudsen diffusion, therefore the hydrogen flux through porous substrate can be expressed as,

$$\mathrm{J_{Total}} = \left[\frac{2}{3}\frac{\varepsilon r}{\tau}\frac{1}{l}\left(\frac{8}{\pi\,\mathrm{R\,T\,M}}\right)\right] + \left[\frac{1}{8}\frac{\varepsilon}{\tau\eta}\frac{r^2}{R\,T\,l}P_{av}\right]\Delta P$$

Equation 6.4

This can be simplified to,

$$\mathrm{J_{Total}} = \left[\alpha_K + (\beta_V P_{av})\right]\Delta P$$

Equation 6.5

This simplified equation enables the characterisation of hydrogen transport across a porous membrane. Both the tortuosity and porosity of a membrane directly affect how well hydrogen flows through a porous membrane, and with experimentally determined α and β values using Equation 6.5, hydrogen flux can be calculated at any given condition of pressure or temperature.

6.2 Hydrogen permeation through a Pd/PSS membrane

Unlike self-supporting membranes, permeabilities for multilayer composite membranes cannot be calculated using the general permeability equation, where ø is the permeability, l the membrane thickness, *Pi* is the external high pressure and *Pint* the internal film-substrate interface pressure (Point V in Figure 6):

$$J_{H2} = \phi \frac{(\mathrm{Pi}_{\mathrm{H2}}^{\mathrm{n}} - \mathrm{Pint}_{\mathrm{H2}}^{\mathrm{n}})}{\mathrm{l}(x)}$$

Equation 6.6

The equation developed by Ward an Dao [16] doesn't account for the different layers. In order to fully characterise the permeability, a theoretical model proposed by Gabitto et al [52] takes into account gas transport at different stages within the membrane, shown in Figure 6.

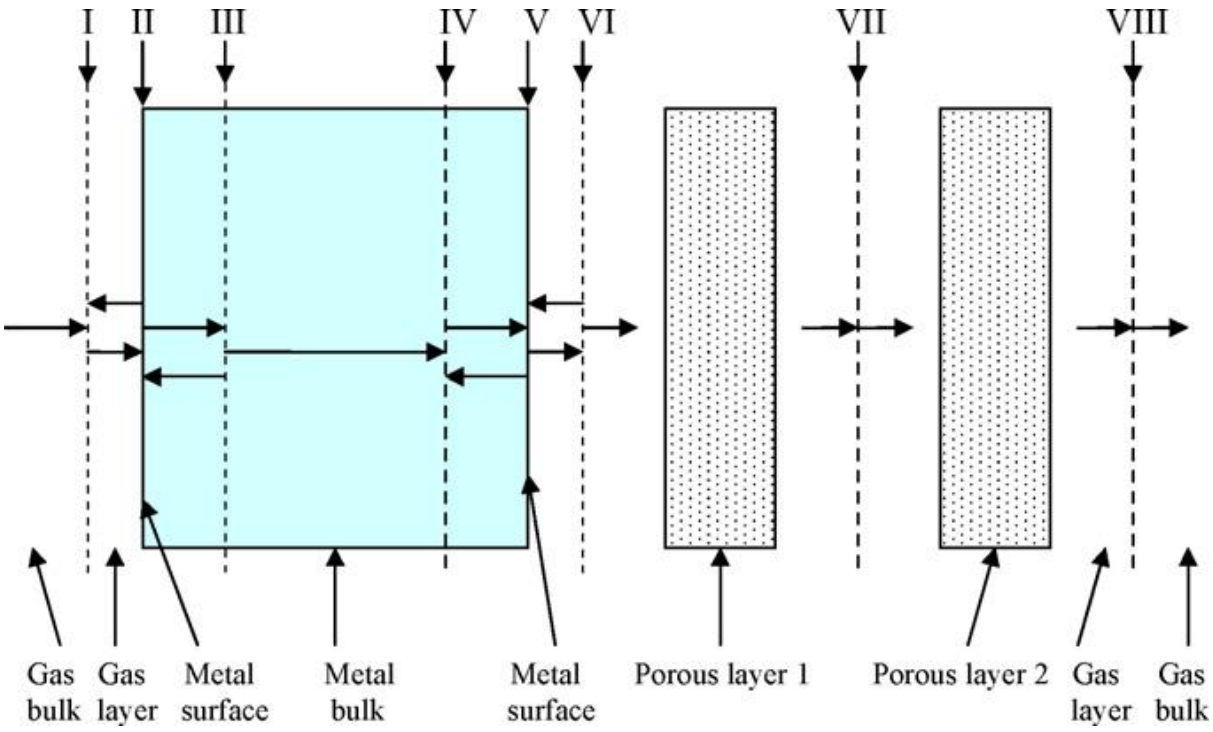

Figure 6- Multi-stage transport model across a 3 layer composite membrane. [52]

The model is largely based on the work carried out by Ward and Dao [16] and Burggraaf [51], and proposes 8 different regions within a 3 layer composite membrane. Regions I-VI cannot be simply calculated using the general permeability equation and therefore a modified version must be used.

Regions VI-VIII are regarded as a single entity in terms of gas flow, even though there maybe differences in structures within the membrane. Through composite structures hydrogen transport is predominantly a combination of both Knudsen diffusion and Poiseuille flow expressed previously as,

$$J_{Total} = \left[\frac{2}{3}\frac{\varepsilon r}{\tau}\frac{1}{l}\left(\frac{8}{\pi\, R\, T\, M}\right)0.5\right] + \left[\frac{1}{8}\frac{\varepsilon}{\tau\eta}\frac{r^2}{R\,T\,l}P_{av}\right]\Delta P$$

Equation 6.7

As explained in the previous section, the equation can be grouped to give α_K and β_K values which are established experimentally. From this hydrogen transport through areas VI-VIII can be evaluated.

Section 7- Thin Film / PSS Interface Layer

7.1 Introduction

To successfully deposit a continuous defect-free layer onto a PSS substrate, as previously stated in Section 5, two main obstacles have to be addressed. Firstly, the surface pore size of the porous substrate must be reduced, but not to an extent where the surface is too smooth for

mechanical adhesion, and, secondly, the interdiffusion of Fe ions into the palladium lattice must be prevented.

In most cases intermediate layers serve to either reduce pore size or to prevent interdiffusion. Layers that have been investigated, include: TiN [53], oxide layers [36], alumina [54], NaA zeolite [55], yttria-stabilised zirconia [10], and tungsten [12]. Only a small number of studies have looked to solve both pore size reduction and the prevention of interdiffusion using a dual-purpose intermediate layer. This section identifies different methods and materials used to modify the PSS surface, and then examines the work by authors attempting to reduce both surface pore size and rate of interdiffusion.

7.2 Surface modification

7.2.1 Pore size reduction

One of the simplest methods adopted to reduce surface pore size is the plastic deformation of the substrate surface using mechanical abrasion. This method was shown by Mardilovich et al [48] to successfully decrease the surface roughness, however the extensive plastic deformation of the surface closed most of the surface pores leading to an almost completely dense layer. This layer was subsequently almost entirely impermeable to hydrogen, highlighting the need to maintain porosity.

Another approach is to fill the PSS pores with a fine sub-micron powder. Tong et al [56] used aluminium hydroxide gel to fill the large surface pores, successfully allowing a 3 μm Pd-Ag film to be deposited onto the surface. However, when tested under elevated temperature above 500°C the aluminium hydroxide was reduced, thus making it more susceptible to pinhole formation and delamination. Surface modification using other sub-micron powders has also been used by a number of groups. Nam et al [57] filled the surface pores with nickel powder

and was again successful at coating a thin membrane layer capable of meeting the DoE Department of Energy's guideline flux target [7]. However, the direct contact between the Pd/Ni coating and the PSS/Ni substrate would ultimately result in intermetallic diffusion at temperatures above 400ºC.

A non-metallic approach was taken by Checchetto et al [21] who devised an original technique using semi-porous polymeric film. This intermediate layer was spin-deposited onto the PSS surface and served to reduce both the surface roughness and the surface pore size. A successful Pd membrane layer of 5 µm was coated onto the modified surface which showed good selectivity values. However, the membrane was only tested under low temperature conditions, thereby highlighting the temperature limitations of the polycarbonate film.

Fletcher et al [19] modified the surface using a novel laser melting technique. They used different strength laser beams to melt the PSS surface, which enabled them to successfully eliminate the large, un-coatable surface pores. The reduction in pore size resulted in a thin 5µm Pd-Y membrane layer being able to be deposited by magnetron sputtering. Despite a very thin layer being achieved, the adhesion of the membrane layer was not successful. Using the laser beam in an atmosphere of air resulted in an oxide layer forming on the surface, which formed an incompatible interface layer which led to delamination of the membrane.

7.2.2 Interdiffusion barriers

The most common method of preventing interdiffusion in composite membranes is to use a porous intermediate layer between the interface of the substrate and the deposited membrane layer. In order for the intermediate layer to be functional, it must be a highly porous structure that does not inhibit the flow of hydrogen through the composite layers. It also must remain chemically stable at operating temperatures from 400-600ºC and is required to be robust enough (e.g. necessary thickness) to prevent any interdiffusion.

Ma et al [58] addressed the interdiffusion problem, by oxidising the surface of the PSS substrate. After heating to temperatures up to 800°C the resultant surface was a combination of Fe_2O_3 and Cr_2O_3. They achieved a range of oxide thicknesses ranging from 1-6 µm, with Cr_2O_3 being most desirable as a diffusion barrier, as it showed high stability when under a hydrogen atmosphere. Ma et al [58] deposited a Pd-Cu membrane layer onto the oxidised PSS, which was found to be stable for over 6000 hours between a temperature range of 350-450°C. The oxidation of the PSS surface additionally helped to increase the adhesion of the Pd-Cu film by providing a relatively rough surface for the film to anchor onto. However, this technique did not address the problem of large surface pore sizes, thus resulting in a thick Pd-Cu film being deposited in order to produce a continuous defect-free layer.

Grayaznov et al [12] utilised the high melting point of tungsten (3410°C) in an attempt to eliminate the thermal expansion mismatch and found that a tungsten intermediate layer was successful at preventing inter-diffusion at elevated temperatures (800°C). However, the thin tungsten layer did not significantly reduce the pore size of the substrate, resulting in a relatively thick (>10 µm) Pd layer being required to produce a pinhole-free layer. Increasing the thickness of the tungsten layer would decreased surface pore size, which would enable a thinner defect-free Pd layer to be coated. However, whilst effective at reducing the size of larger pores, this may also adversely fill in the smaller pores diminishing the overall hydrogen permeability.

Huang & Dittmeyer [10] coated pure Pd onto an yttria-stabilised zirconia (YSZ) interdiffusion layer supported by a porous stainless steel substrate. Their results showed that the ceramic YSZ layer effectively eliminated interdiffusion up to 600°C. Not only did the YSZ barrier show good hydrogen permeability, with the potential to be further optimised, it also

performed well in the adhesion tests. However tests need to be carried out at temperatures above 600°C to further investigate its durability under membrane reformer conditions.

7.2.3 Combination of both surface modifications

In an attempt to address both problems caused by surface pore size and intermetallic diffusion, Li et al [59] combined the surface abrasion technique with the powder filling process used by Nam et al [57]. The two-stage process began with an abrasion technique similar to that used by Mardilovich et al [48], however it was proceeded by an acid etch. This served to re-open some the pores that would have been closed during the abrasion, seen in Figure 7- SEM images of multistage PSS substrate surface preparation sequence as used by Li [59]. a) As-received PSS, b) Surface abrasion, c) Acid etch to re-open pores, d) Pore-filling with 2.5 μm α-alumina powder, e) Final pore-filling with 0.3 μm α-alumina powder. from stages (b-c). The second stage, shown in Figure 7 (c-d-e), deposited α-alumina powder in two different stages using a sol-gel technique. A powder coating of 2.5 μm particle size was firstly deposited (c-d) and secondly a 0.3 μm layer (d-e). This process proved to be successful at reducing the pore size and resulted in a membrane layer thickness of only 5 μm being deposited.

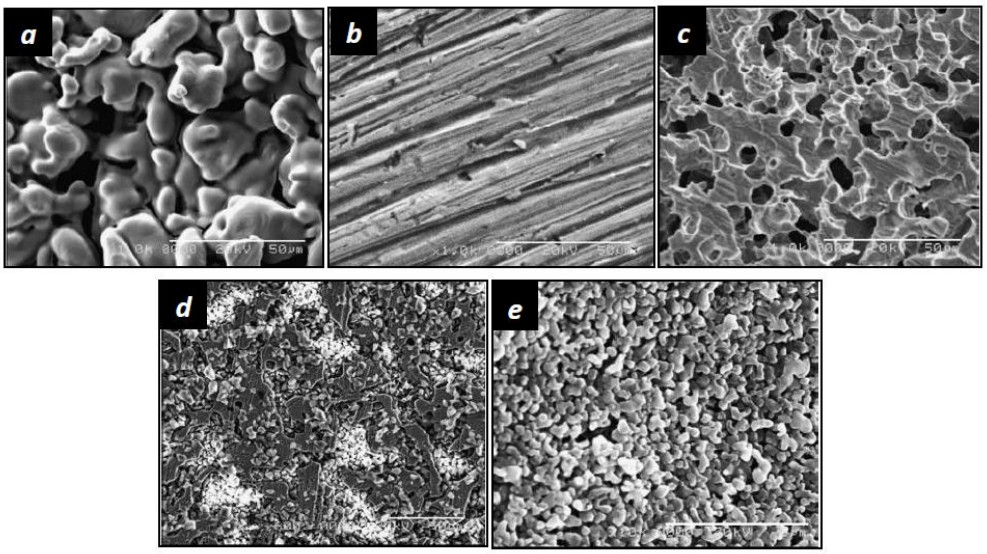

Figure 7- SEM images of multistage PSS substrate surface preparation sequence as used by Li [59]. a) As-received PSS, b) Surface abrasion, c) Acid etch to re-open pores, d) Pore-filling with 2.5 µm α-alumina powder, e) Final pore-filling with 0.3 µm α-alumina powder.

When tested for its ability to prevent interdiffusion it was successful up to a temperature of 650°C. Although successful in both reducing pore size and preventing intermetallic diffusion, this membrane still suffers from the same issues as a porous ceramic substrate, in that, delamination and membrane failure due to the thermal expansion mismatch still exist due to the ceramic-metallic interface. Therefore, thermal cycling, which is typically experienced in membrane reactors, will undoubtedly cause delamination of the membrane [60].

It is clear that most of the past research has focussed solely on one of the two issues facing composite thin film membranes. Whilst it is clear that a number of groups have been successful in either reducing the pore size of the substrate, or reducing interdiffusion between the substrate and the Pd-based membrane, there is a clear gap in the literature successfully combining the two. If PSS composite membranes are to going to be utilised within a membrane reactor and meet the DoE hydrogen flux targets [7], these two issues need to be both addressed.

Section 8- Project aims

The primary aim of this project is to investigate the dual performance of a sub-micron tungsten powder intermediate layer to perform both as a medium to reduce pore size and to prevent intermetallic diffusion.

The extent of the powder filling and surface pore reduction will be calculated along with the effect on hydrogen transport through the modified substrate. Using layers of both Pd and PdCu, this project will also examine the performance of a tungsten intermediate barrier on its ability to prevent iron diffusing into the Pd/PdCu membrane layer.

Chapter 3 – Experimental

Section 9- Experimental techniques

9.1 Introduction

This chapter is divided into 3 sections. The first section gives details about the substrate material and an account of the sample preparation and membrane production method. The second section presents sample characterisation, in terms of surface topography, surface morphology and membrane structure. The last section provides details on the gas permeation apparatus and procedure.

Section 10- Materials and Sample preparation

10.1 Porous substrates

Discs of porous 316L stainless steel (PSS) from Mott Metallurgical Corporation (USA) were used as the substrate. This porous stainless steel (PSS) substrate had a thickness of 1 mm, a diameter of 21mm and a media filtration grade of 0.1µm. The filtration grade is calculated and defined as the minimum size of a hard spherical particle retained by the interconnected porosity [61], with 0.1 µm being the smallest commercially available grade.

All the discs were firstly cleaned with acetone using an ultrasonic bath. After 15 minutes of cleaning the sample discs were taken out and dried using a heat gun to ensure any residual acetone had evaporated prior to use. Whilst handling samples, latex gloves were used at all times in order to minimise contamination.

10.2 Tungsten intermediate layer

Tungsten powder with a sub-micron particle size was obtained from Sigma-Aldrich.

Step 1: Place stainless steel disc onto a vacuum pad.

Step 2: Disperse one heaped spatula of tungsten powder into 10 cm^3 of Industrial Methylated spirit (IMS) and stir. This facilitates the handling and coating of the powder.

Step 3: Apply vacuum to the underside of the PSS disc and coat an even layer using a very fine bristle paintbrush.

Step 4: If there is clearly an excess of powder particles on the surface, very carefully dust-off the excess powder.

10.3 Heat treatment

The treated discs were then carefully wrapped in stainless steel foil and placed into a vacuum furnace at 900°C for 2 hours under a vacuum of approximately 10^{-4} mbar. After which they were left to cool over a period of 12 hours. The samples were then taken out and any excess tungsten was lightly dusted off the surface with a 'gas duster' containing fluorocarbon (usually used for cleaning electronic equipment).

10.4 Thin Film: Magnetron Sputtering

Films of varying thickness (5, 10, 20, 30 µm) of 316 stainless steel, and 2- 5 µm films of palladium and palladium copper, were deposited onto disc-shaped samples of PSS+ W. The DC magnetron sputter deposition and sputtering source targets were sourced through Teer Coatings ltd. The target to substrate distance was kept constant during deposition and the same sputtering gun was used for all depositions. Immediately before deposition, the sputtering chamber was evacuated to approximately 10^{-6} Mbar and then back-filled with ultra

high-purity (UHP) argon. Prior to deposition, the samples were subjected to a final ion cleaning stage using an argon plasma.

The alloy film (PdCu) was coated via co-deposition using a single Pd target (99.9 % purity) and a Cu target (99.9 % purity) for 1800 seconds. The targets were mounted next to each other in order to produce a fully homogenous solid solution layer, and to further aid homogeneity the samples were rotated inside the chamber at 8 rpm. The films were deposited using a range of different powers supplied to each target in order to replicate as near to the desired 60:40 percent atomic ratio of palladium to copper.

The power supplied to the Pd target was set at 250 W so that the thickness of the films could be accurately controlled. To vary the thickness of the deposited Pd film different coating times were used. A coating time of 1800 seconds was used to give a 2 µm layer. To measure the thickness of the coated films a glass slide was also fixed into the sputtering chamber alongside the PSS+W samples. The precise thickness of the Pd coatings was determined by measuring the step difference between the top of the coating and the substrate, using an Olympus LEXT confocal laser microscope.

Section 11- Material characterization

11.1 Scanning Electron Microscopy and EDX analysis

Surface morphologies of the composite membranes and as-received samples were examined under a scanning electron microscope (JEOL SEM 6060) at various stages of the experimental process. This gave a visual representation of the amount of tungsten being deposited and to what extent the pores were being filled.

Analysis of the degree of interdiffusion was carried out by tracking the amount of Fe that diffused into the palladium / palladium copper surface layer, using INCA EDX. A line was drawn that started in the PSS disc and went through the tungsten layer and into the Pd membrane. The EDX software was able then to show the composition of different elements found along this line. This gave a graphical representation of the extent of the interdiffusion taking place.

11.2 X-ray Diffraction

The structure of the deposited films, in terms of their composition, was analysed using a Bruker D8-Advance diffractometer using monochromatic $CuK\alpha_1$ radiation (λ = 1.54056 Å). This piece of equipment uses Bragg's law to analysis the diffraction patterns,

$$\text{Bragg's law} = \lambda = 2d_{hkl} \sin\theta$$

Equation 11.1

Where λ is the wavelength, θ is the angle of incidence of diffraction and d_{hkl} is the inter-planar spacing. The alloy composition was calculated using the lattice parameter, a using the equation below, where h, k and l are the miller indices;

$$d_{hkl} = a/\sqrt{h_2+k_2+l_2}$$

Equation 11.2

Section 12- Material surface metrology

12.1 Confocal laser microscopy

The Olympus LEXT OLS 3100 mounted on a TableStable anti-vibration table was used to gather accurate measurements of pore depth, pore volume, step profiles, surface roughness and film thickness. The microscope uses a 408 nm class II ultraviolet laser source and has a plane resolution (X and Y) of 120 nm and a space pattern (z resolution) of 10 nm. It uses a series of 'stacked' confocal images along the z-axis and as the laser is reflected off a surface it is passed back through the objective and converged on a second point, which is objectively conjugate to the first. With a circular pinhole ensuring only light from the focal plane is detected, an optical section is generated. Further increments of 5-100 nm along the z-axis create additional optical sections at high or lower planes. These sections are then stacked together to produce a 3-D image which gives accurate details of the metrology of the composite membrane [19]

12.2 Membrane permeability

To assess the gas flow measurements a specially made membrane rig was used. The gas tight chamber was made from a single piece of Inconel 625 grade II alloy, and was secured to the base via a silver compression gasket. This rig fundamentally measures the gas that permeates through a membrane, by applying a controlled feed gas to the high-pressure side of a fully sealed membrane and measuring the amount of gas flowing into the low-pressure side. The PC software SpecView was used to control and log all the essential data, including pressure, temperature and hydrogen flux.

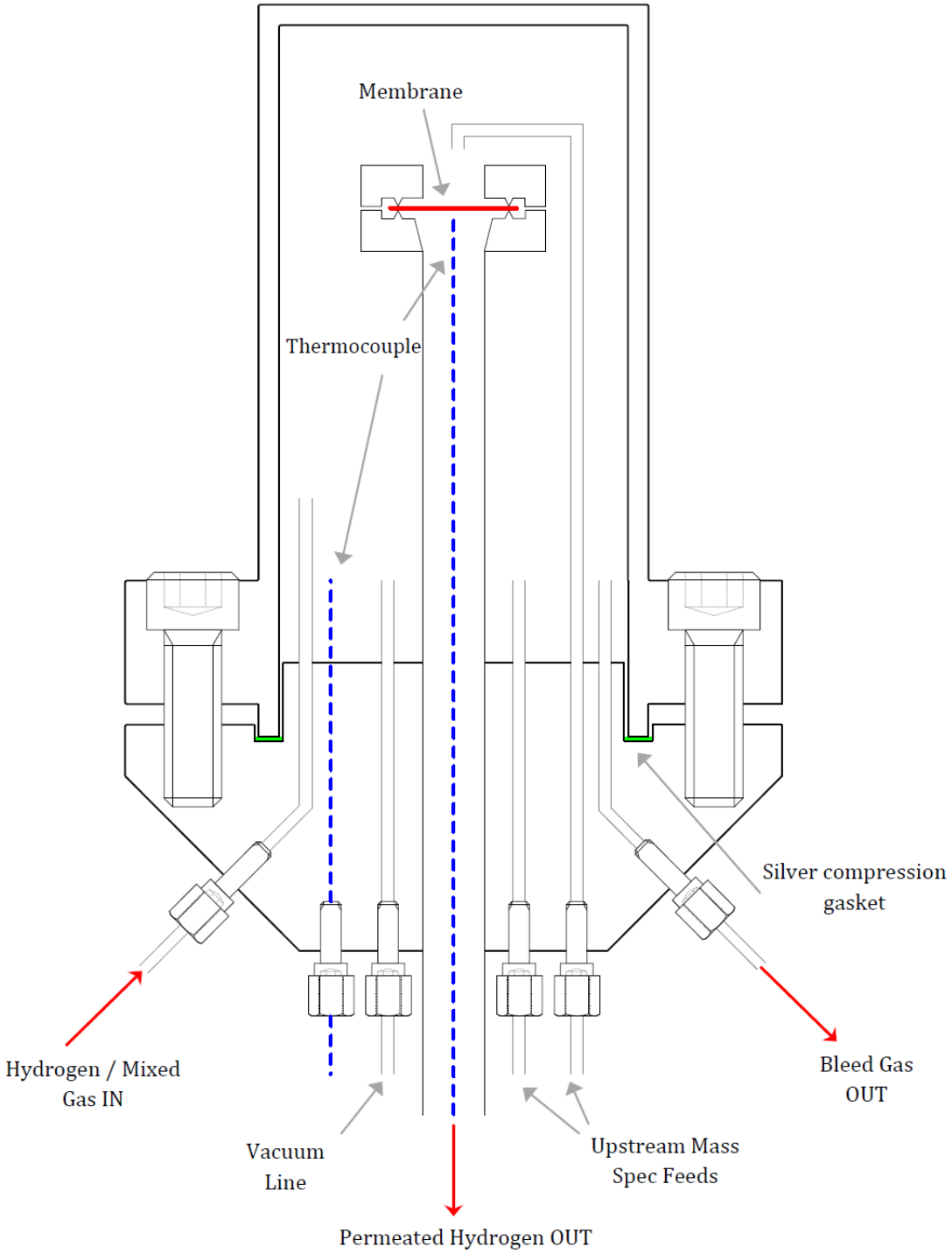

Figure 8-Schematic diagram of the membrane reactor vessel. (Not to scale) [19]

The gases used in this project were ultra-pure BIPS hydrogen (99.99995 %) and nitrogen (99.95 %) with the hydrogen supplied by Air Products and the Nitrogen by BOC. They were regulated using two Brooks Mass Flow Controllers (MFC) calibrated over a range of 6-600

$ml.min^{-1}$. The gases were supplied into the high-pressure side of the rig, to insure that any contaminates that were blocked by the membrane surface were bled away. To ensure a constant pressure within the chamber a bleed MFC was also used to accurately control the feed gas between pressures of 100 -1100 ± 0.005 (bar) On the low-pressure side the amount of gas flowing through the membrane was measured using a Brooks 5850S MFC calibrated for different flow rates. For the purpose of this project, the MFC with a range of 6-600± 6 $ml.min.^{-1}$ was used for the high fluxes and if the flux range was expected to be >200 $ml.min.^{-1}$ then a different MFC would be used. Attached to the membrane chamber on both the up- and down-stream side was a Pfeiffer TSU-071-E turbomolecular drag pumping station (with a membrane backing pump) capable of producing a vacuum of 10^{-7} mbar.

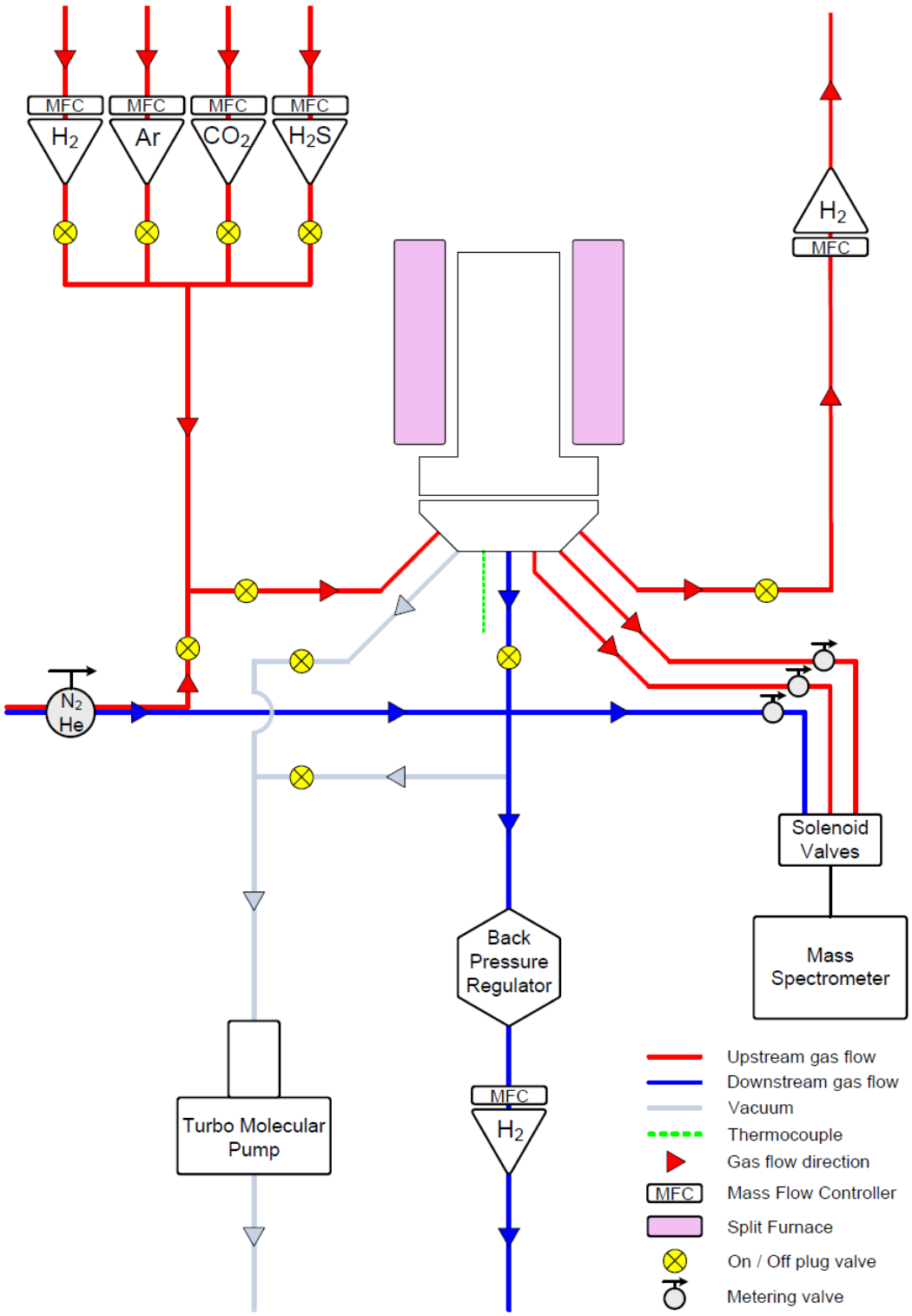

Figure 9- Schematic diagram of the hydrogen permeation system [19]

To fully secure the sample membranes, two hardened 316N stainless steel CF vacuum flanges with a hard knife-edge were used to clamp the membrane. Each flange had a hole bored with a 12.7 mm diameter, with one of them being welded to the end of a ½" tube and the other acting as a 'cap' to provide the clamping force necessary to prevent gas leaks. To establish the gas-tight seal, Cu gaskets were used on each side of the sample membrane. The softer metal could be uniformly deformed around the hard knife-edge as the two flanges were tightened together using low thermal expansion hex bolts.

Once the gas-tight seal had been established both the up- and down-stream sides of the rig were evacuated to around 10^{-5} mbar. This served to flush out any unwanted gases before hydrogen was then allowed to flow into both sides of the membrane. Once equilibrium had been reached, measurements could then proceed.

The permeabilities of the membranes in this project were measured at three separate stages with both hydrogen and nitrogen. The as-received (A-R) PSS were tested first, the second test was carried out after coating with either 1 or 3 layers of tungsten, and the third stage measured the effect of 5, 10, 20, 30 μm layers of stainless steel.

Chapter 4 - Results & Discussion

Section 13- Introduction

13.1 Introduction

This section will examine the effects of tungsten powder pore-filling and how it affects the reproducibility of a continuous defect-free stainless steel (SS) layer. SEM images will provide a visual representation of the overall surface coverage of the powder, the confocal 3D microscope will enable analysis of the extent of pore-filling and the membrane test rig will assess the permeability of the samples, showing the performance of the SS layer in terms of pinholes and defects within the layer.

The second section will examine how the tungsten intermediate layer performs against intermetallic diffusion. Cross sections of the coated PSS were examined using EDX software to track interdiffusion between the porous stainless steel substrate and the Pd/PdCu layer.

Section 14- Porous Substrate

14.1 Introduction

In order to directly compare the findings of this study, the PSS discs used replicate those used in previous studies [56, 57, 62]. The sintered austenitic 316L stainless steel (PSS) discs (21 mm diameter, 1 mm thickness), purchased from Mott Corp were fabricated by stamping the porous sheet material. All the discs used had the smallest commercially available grade pore size (0.1µm) and were from the same batch to insure continuity.

14.2 Structure and topography

14.2.1 As-Received PSS

The 0.1µm value is not an indication of the average pore size; rather, it represents the minimum size of a hard spherical partial held within the interconnected porosity [61]. The average surface pore size of the disc is between 10-20 µm, with the largest pore being in the region of 30 µm and the smallest being less than 5 µm. According to a rule put forward by Ma et al [28], which suggested that a membrane layer needs to be 3x the size of the largest surface pore, the AR-PSS (Figure 10) is not suitable for the direct deposition of a thin membrane layer. The surface topography of 316L porous stainless steel (PSS) is shown in figure 10.

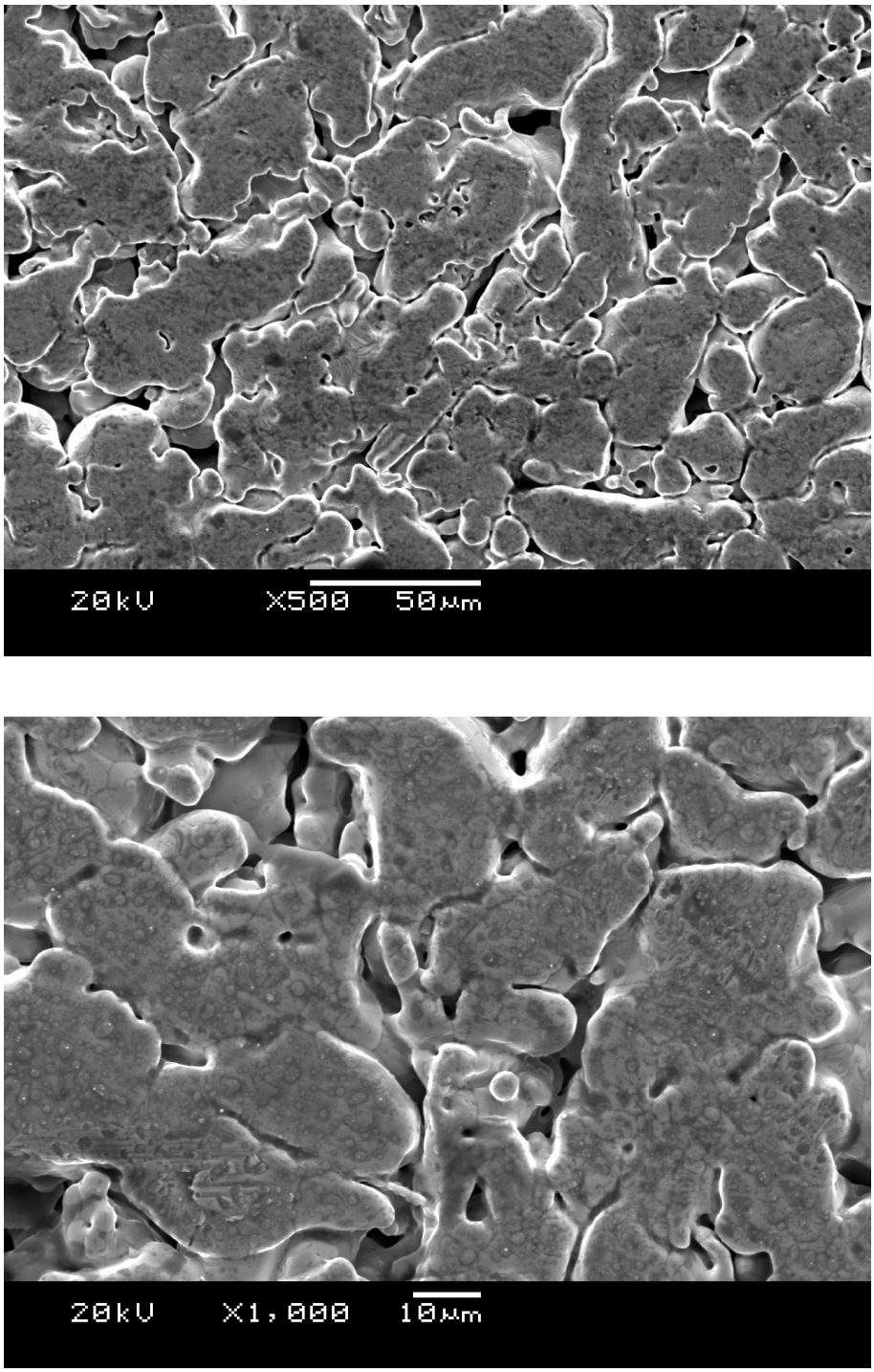

Figure 10- SEM images of the surface topography of as-received PSS, showing surface pore sizes ranging between 5 and 30 µm.

In order to accurately quantify the surface topography, a 3-Dimensional image was taken using an Olympus LEXT confocal laser microscope. The resulting image, shown in Figure 11, clearly demonstrates the extent to which pore-depth can vary with the larger pores possessing

depths up to 13 µm and the smaller pores a depth 2 µm. The variation in pore-depth and size is a characteristic that inhibits the deposition of a thin film membrane; therefore the surface pore size needs to be reduced whilst still maintaining a high level of porosity.

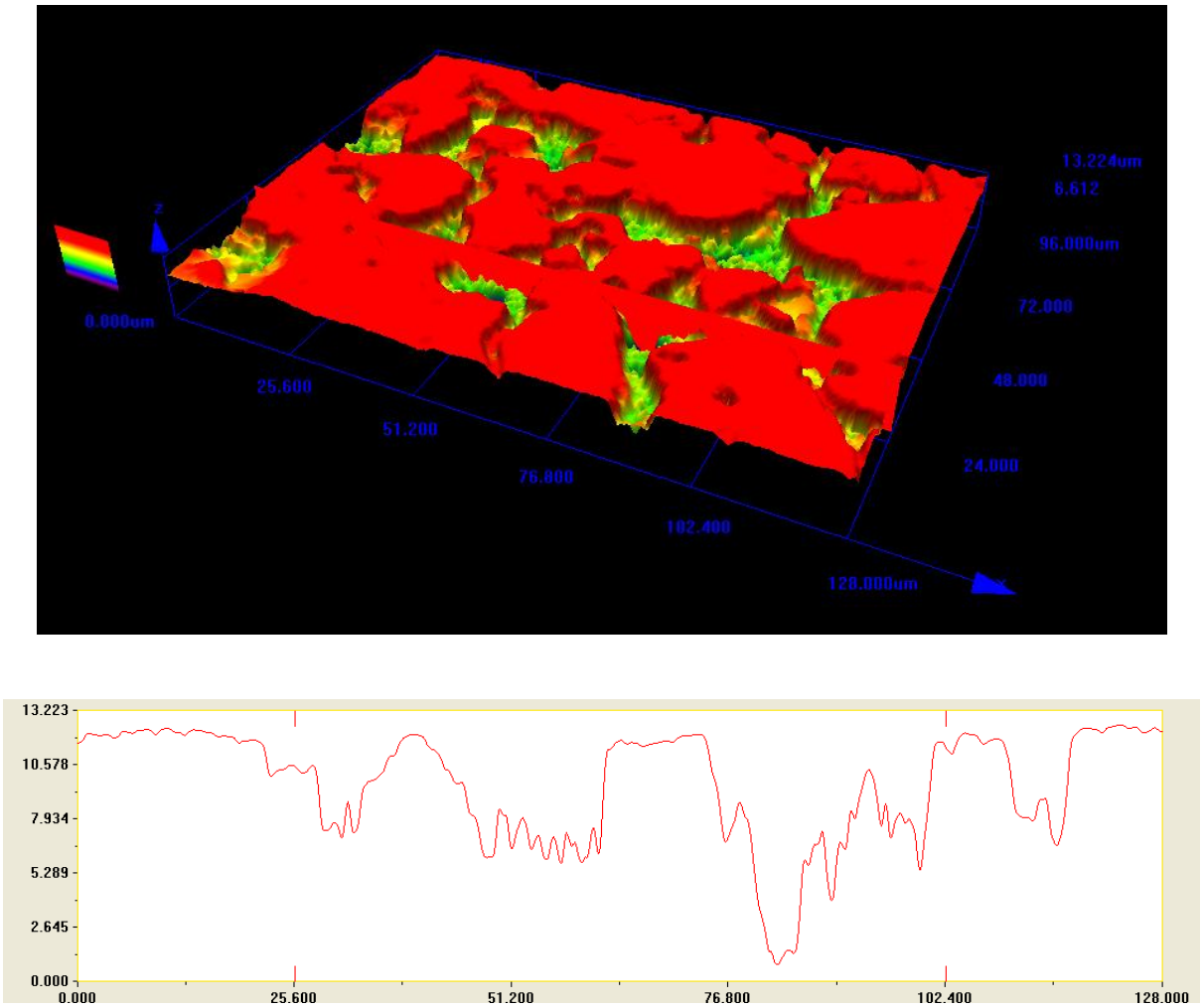

Figure 11- Confocal laser microscopy image of A-R PSS surface topography with line profile (µm).

Section 15- Stainless steel coated PSS

To demonstrate the unsuitability of an untreated PSS disc for depositing a film thin enough to meet the US DoE targets (> 5 µm), stainless steel was sputtered onto the surface. The PSS disc in Figure 12 has been coated with 5 µm of stainless steel from a single 316 target. The under-lying structure remains visible with large pores prominent and only the very small surface pores being covered. The large surface pore structure of PSS is clearly not suitable as a mechanical support for depositing thin film membranes.

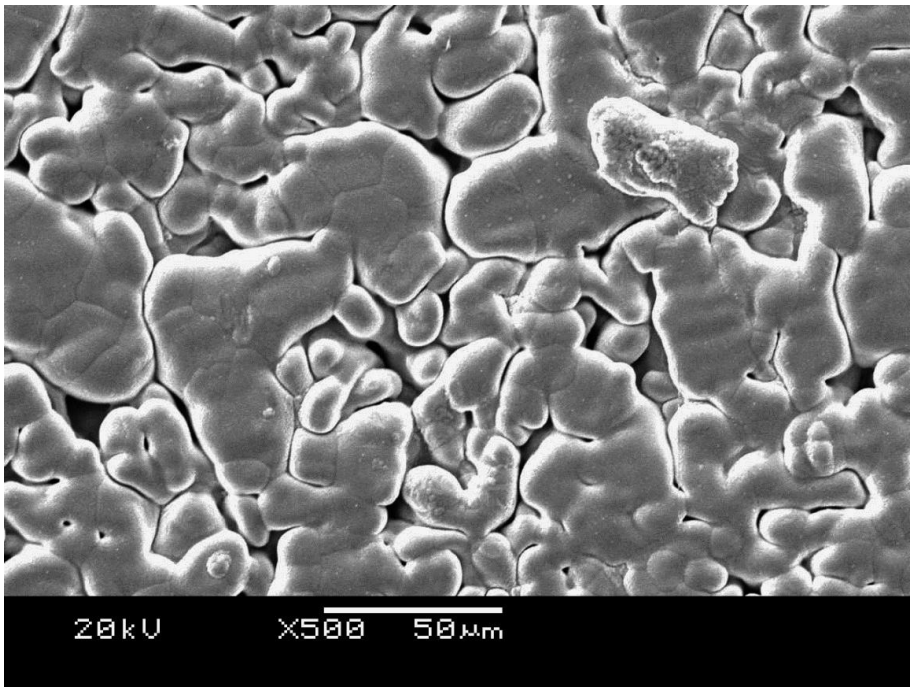

Figure 12- SEM image showing the effect of SS coating thickness on the surface pore size of as-received PSS

Section 16- Tungsten powder deposition

As mentioned in the previous section, A-R porous stainless steel discs are unsuitable as a substrate material for depositing thin film membranes. The large pore size precludes the deposition of a continuous, defect-free thin film membrane; therefore the surface must be modified in order to reduce the pore size.

16.1 Tungsten powder

Modification of the PSS discs was implemented by depositing submicron tungsten powder onto the PSS surface. Figure 13 shows that there is a slight variation in particle size, however the large majority are >1 μm in size.

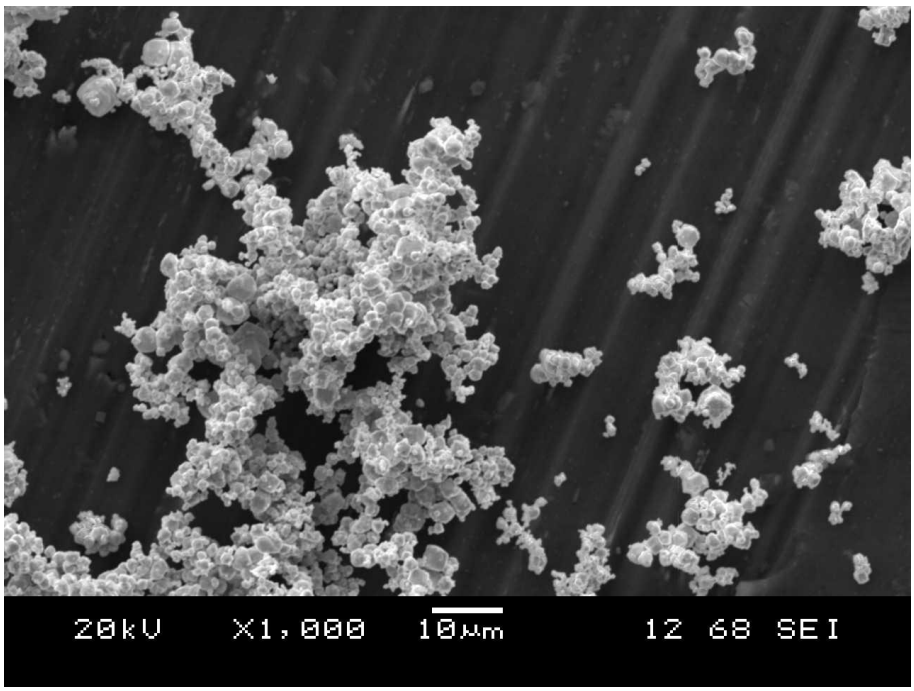

Figure 13- SEM secondary electron image showing the size of the tungsten powder particles.

In total 16 samples were coated, 8 coated with a single layer of tungsten and 8 coated with 3 separate layers of tungsten. After each successive layer of tungsten powder the coated disc was then placed into a low vacuum furnace (10^{-4} Mbar) and sintered at 900°C for 2 hours.

16.2 Coating without a vacuum

The powder tungsten was firstly coated onto the PSS without the use of a vacuum on the underside of the disc. This technique was not successful in fully filling the surface pores with the desired amount of powder. Due to the nature in which the powder was coated, the particles of tungsten were not being drawn into the pores, and thus a large proportion of the

particles resided in and around the surface of the pores, as shown by the black arrows in Figure 14.

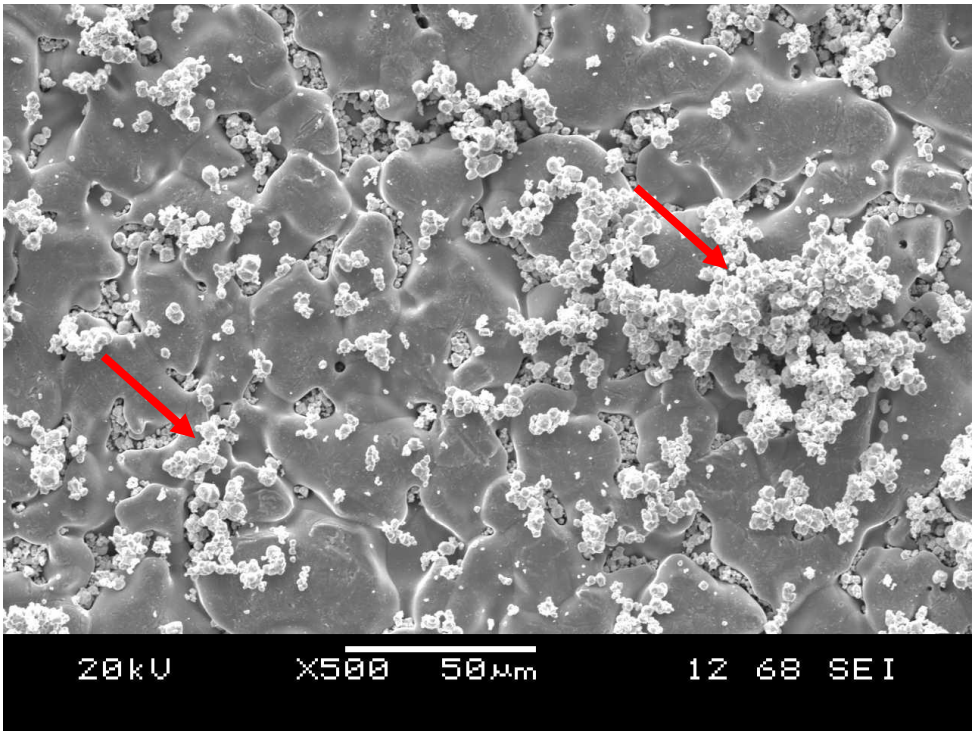

Figure 14- SEM secondary electron image showing the extent of 1 layer of tungsten powder pore-filling without a vacuum

16.3 Coating with a vacuum

In order to increase the amount of pore-filling and to eliminate surface deposition a vacuum was used on the underside of the PSS disc. This served to draw more of the tungsten from and the surface and into the pores.

SEM images in Figure 15 give a visual representation of the effectiveness of the vacuum, showing a significant improvement in pore-filling and a decrease in particles residing on the surface.

Figure 15 also shows clearly the difference in the two coatings. Whilst both show to have a fairly even coverage across the disc, the 3 layer clearly has a greater amount of tungsten

deposited within the pores. Therefore, it is evident that the number of coating times positively correlates with the amount of tungsten deposition.

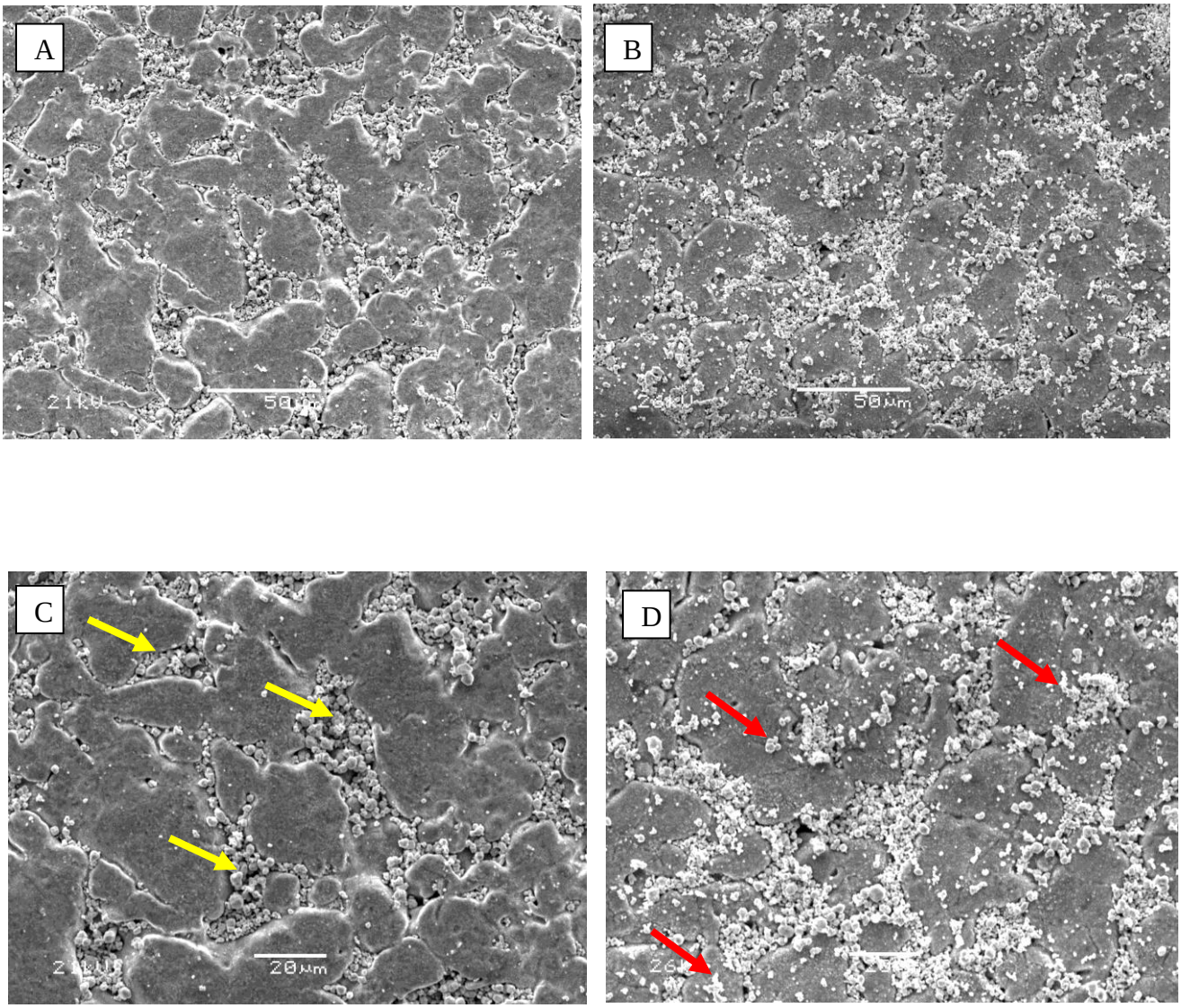

Figure 15- SEM secondary electron images showing - A=1 layer of W powder, B=3 layers of W powder, C= 1 layer of W powder, and D= 3 layers of W powder (all deposited with a vacuum).

In images A and C it can be seen that the applied vacuum used on the underside of the disc has enhanced pore-filling by drawing the tungsten particles into the surface pores, as shown by the black arrows. However, in images B and D, tungsten particles have started to reside on the surface. Although the vacuum has been effective at drawing the particles into the pores, the increased amount of tungsten has resulted in the pores becoming overfilled; this is shown

by the red arrows. It is evident that as coating cycles increase from 1 to 3, clumps of tungsten powder start to accumulate on the surface as the pores become filled. Clumping of the tungsten creates a rough uneven surface profile which hinders the deposition of a continuous membrane layer; however a small amount of surface roughness might actually help with the adhesion of the sputtered layer [40].

When comparing the line profiles of Figure 11 (A-R PSS) and Figure 16 (1 layer of tungsten) it is clear that the Tungsten layer has significantly modified the surface by reducing the pore depth by an average of 50 %. The A-R sample had a maximum pore depth of 13 µm and an average of 8 µm, whereas the tungsten treated sample has an average pore depth of 4 µm.

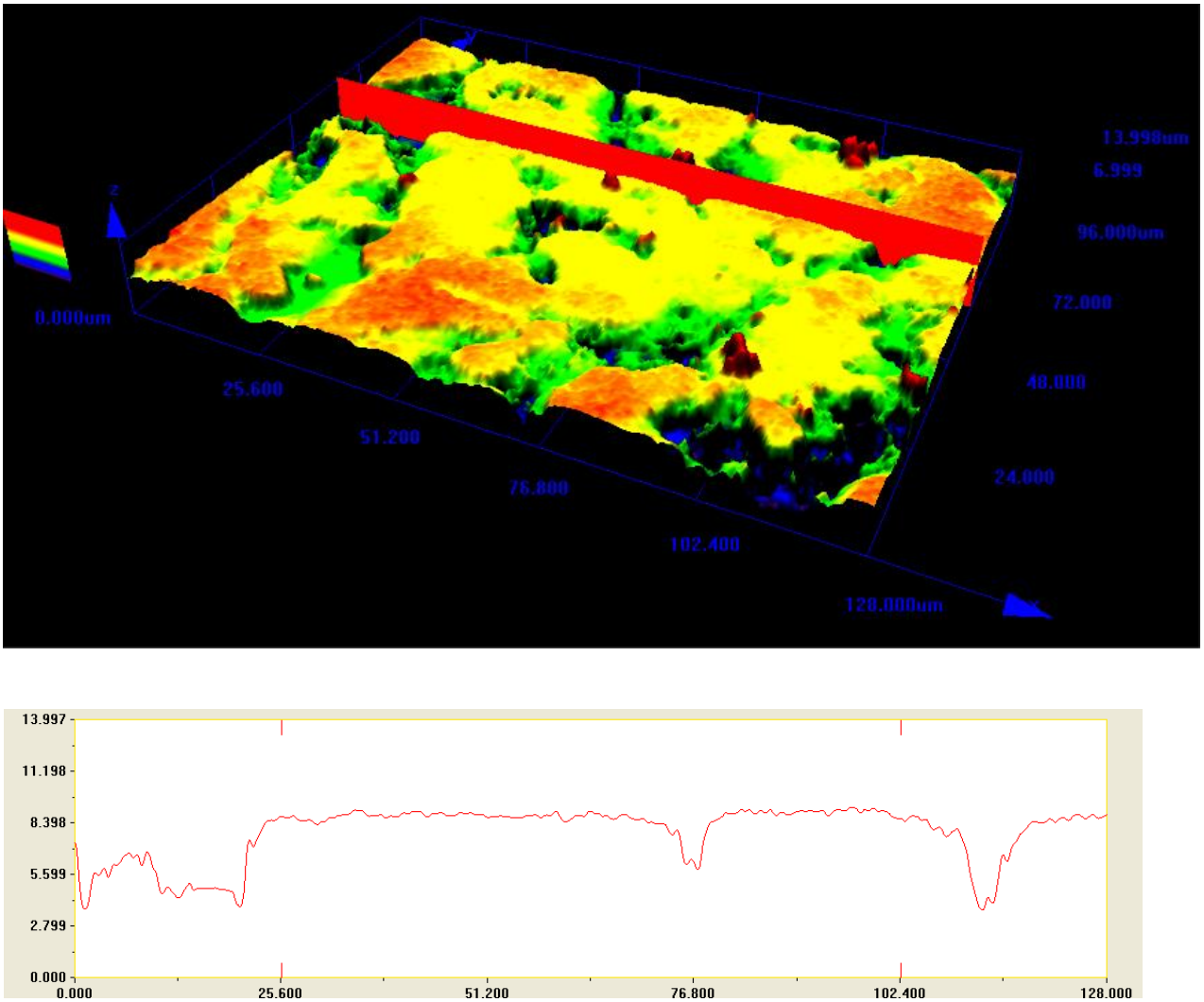

Figure 16- Confocal laser image of AR-PSS modified with 1 layer of <1 µm tungsten powder showing extent of pore-filling.

The confocal image and line profile in Figure 16 shows that the tungsten deposition is fairly uneven with not all the pores being filled equally, for example the pore in the bottom right hand side has significantly less deposition compared to other areas of the sample. However when compared to the surface of Figure 17 which has 3 layers of tungsten, there is a significantly greater amount of pore filling with most pores being filled and a maximum pore depth of 2µm. The greater amount of tungsten deposited onto the surface has resulted in the

surface becoming very rough in nature due to powder clumping. This will undoubtedly affect the continuous nature of any subsequent membrane layer in the same way a large pore would as the profile is reversed. Therefore, the underlying surface needs to fill the pores without overfilling, in order to produce a thin defect-free layer.

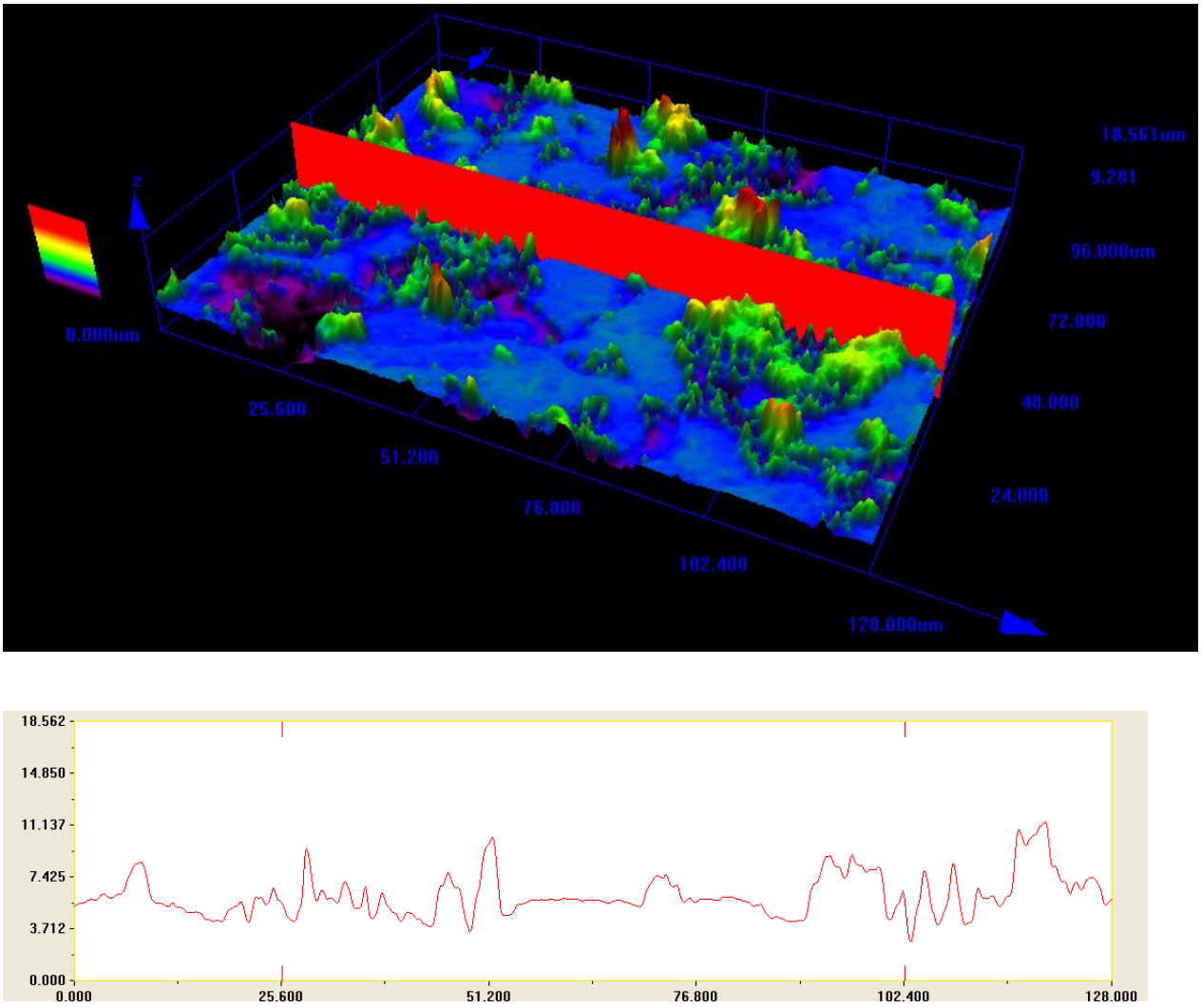

Figure 17- Confocal laser image of AR-PSS modified with 3 layers of <1 µm tungsten powder showing extent of pore-filling. With the red line showing where exactly the cross section was taken.

Section 17- Gas permeability measurements

17.1 Introduction

As discussed in Section 16, microscopy analysis of the W-coated samples revealed a significant reduction in surface pore size compared to as-received PSS. However, in order to understand how the layer is modifying the surface, there is a need to consider hydrogen permeability data. This data should allow the effect of the 1 and 3 coatings of tungsten to be quantified, in terms of the surface porosity, pore size and flux. As mentioned previously in section 6 the total hydrogen flux, *J*, across both substrates types may be expressed as the sum of Poiseuille flow and Knudsen diffusion

$$J\,Total = [\alpha K + (\beta_V P_{av})]\Delta P$$

Equation 17.1

Assuming a linear pressure drop across the substrate, the values of α_K and β_V can be calculated using the experimentally determined values of *J* total hydrogen flux, P*i* and P*ii* which represent the partial pressure gradient. The α_K and β_V coefficients which represent the Knudsen and Poiseuille permeation coefficients, respectively, enable the calculation of gas flux, as a function of temperature and pressure. Therefore, to fully characterise the hydrogen transport across the samples, the α_K and β_V coefficients need to be calculated.

17.2 As-Received Porous Stainless Steel (PSS)

Hydrogen permeability measurements of 16 PSS discs were performed at room temperature. Each disc was taken from the same commercial grade 0.1 μm batch and all exhibited similar average surface pore sizes.

Although the discs exhibited very similar surface pore sizes, there was a large variation in permeability; Figure 18 shows the room temperature permeance of 4 discs, which are representative of the batch. Discs 16 and 2 refer to the upper permeance range, while disc 1 represents more of the average range, and disc 11 shows the lower range.

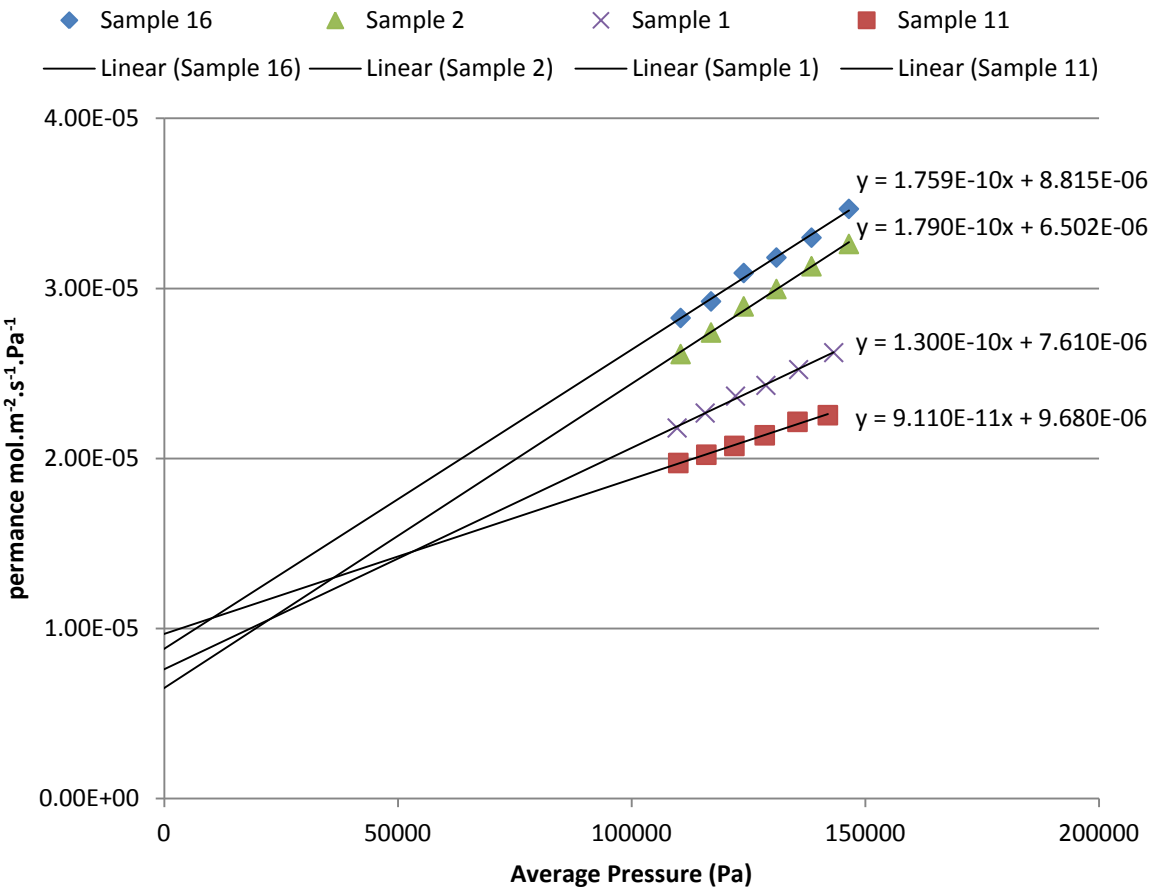

Figure 18- Variation in room temperature hydrogen permeance through as-received 0.1 µm PSS substrates, showing both α_K and β_V coefficients.

When comparing the αK and βV coefficients of the 4 representative discs plotted in Figure 18, it is clear there is a large difference of 48 % between the upper and lower extremes. In order to explain this difference in permeance, the geometric factors ε, τ and r must be calculated.

For simplicity, the numerical parameters in Equation 17.2 may be combined to give the following expressions for αK and βV,

$$\alpha_K = 1.06 \frac{\frac{1}{l}\frac{\mathcal{E}}{\tau} r}{\sqrt{RTM}} \pi r^2$$

Equation 17.2

$$\beta_V = 0.125 \frac{\frac{1}{l}\frac{\mathcal{E}}{\tau} r^2}{\eta RT} \pi r^2$$

Equation 17.3

Of the terms in Equations 17.2 and 17.3, *R*, *T* and *M* are constants whilst αK and βV are determined experimentally. Therefore, an expression for the average pore size, *r*, can be derived [24].

$$r \left[8.48\eta \left(\frac{RT}{M} \right) \right] 0.5 \left(\frac{\beta_v}{\alpha_K} \right)$$

Equation 17.4

The data listed in Table 2 demonstrates that the average pore size, r (0.248-0.877 μm) of the selected samples is well below that of the average surface pore size (10-15 μm). This is in good agreement with Mardilovich et al [63] and a number of other authors who found that the average pore size of the substrate was significantly smaller than that of the surface pore size[59].

Table 2-Comparison of the hydrogen permeance coefficients and geometrical factors a random selection of as-received 0.1µm PSS substrates

Sample:	αK **(mol.m^{-2}.s^{-1}.Pa^{-1})**	βV **(mol.m^{-2}.s^{-1}.Pa^{-2})**	**r (µm)**	$\varepsilon\tau$	**Flux @ RT & 1 bar ΔP (ml/min)**
Sample 1	8.54E^{-06}	1.42E^{-10}	0.45	1.13	682.9
Sample 7	1.31E^{-05}	1.51E^{-10}	0.30	2.90	825.8
Sample 10	5.59E^{-06}	1.87E^{-10}	0.88	0.42	769.2
Sample 11	9.68E^{-06}	9.11E^{-11}	0.25	2.60	540.1

The disc with the largest average pore size would normally be expected to exhibit the highest permeance; however it can be seen that this is not always the case. Table 2 show's that sample 10, which possesses the largest pore size, does not have the largest flow of hydrogen. In order to explain this, the ratio between tortuosity and porosity must be examined. Tortuosity is defined as the increase in distance a molecule must travel when compared to the substrate thickness due to the tortuous nature of the structure. The porosity is defined as the fraction of the media in any particular plane that is open space. Although these two parameters are not directly measurable, it is possible to calculate the average values across the whole substrate from the experimentally determined α_K and β_V values, which are shown in Equation 13 and Equation 14.

It can be seen that the ratio of porosity : tortuosity in sample 10 is low, showing that the underlying bulk porosity significantly resists gas flow even though the surface pore size is relatively large.

17.3 PSS + Tungsten powder

This Section aim's to characterise the effect of the tungsten powder intermediate layer on the hydrogen permeance of the substrates. The 16 discs were coated with sub-micron powder with 8 discs coated with 1 layer and 8 coated with 3 layers. After 2 hours at 900°C in a low (10^{-4} Mbar) vacuum furnace the samples were then tested on the membrane rig in both hydrogen and nitrogen atmospheres.

The permeability data showed that after tungsten coating there was a reduction ranging from 8-25 % in permeance between the As-R samples and the coated samples. Table 3 shows the percentage reduction of hydrogen flux after samples have been coated with 1 layer and Table 4 gives data after 3 layers. When compared to the As-R discs there is roughly a 10 % decrease in flux after 1 layer of tungsten has been applied and an average of 18 % after 3 layers. Interestingly the consistency of the tungsten layer is highlighted, with 1 layer showing to reduce the flux by a more consistent amount in each sample, whereas after 3 layers it is not as consistent with percentage reduction in flux varying from 8 to 25 %. Sample 12 shows a reduction in flux of only 8 %, while sample 8 lowers the flux by 25 %. This, 17 % difference shows that after 3 layers the tungsten powder is not reducing the flux as consistently as had hoped for.

Table 3- Hydrogen flux data before and after 1 tungsten coating at RT and 1 bar ΔP (ml/min) and percentage reduction in flux

Sample: (number of tungsten layers)	AR flux (ml/min)	Flux after W coating (ml/min)	Percentage reduction flux @ RT & 1 bar ΔP (ml/min)
Sample 2 (1W)	761.2	681.7	10 %
Sample 14 (1W)	639.4	585.6	8 %
Sample 10 (1W)	769.2	682.1	11 %
Sample 1 (1W)	682.9	622.2	9 %
Mean	713	642	9.5%
Standard deviation	62.7	47.4	1.29

Table 4- Hydrogen flux data before and after 3 tungsten coating at RT and 1 bar ΔP (ml/min) and percentage reduction in flux

Sample: (n^o of tungsten layers)	AR flux (ml/min)	Flux after W coating (ml/min)	Percentage reduction flux @ RT & 1 bar ΔP (ml/min)
Sample 11 (3W)	540.1	428.0	20 %
Sample 12 (3W)	600.4	557.5	8 %
Sample 9 (3W)	564.9	450.8	20 %
Sample 8 (3W)	731.8	545.8	25 %
Mean	609.3	495.5	18.3%
Standard Deviation	85.3	65.4	7.2

The difference in flux between the AR sample and coated sample is shown to be relatively small for both layers with a maximum reduction of 25 %. This suggests that the tungsten layer is not having a significant effect on H_2 transport through the surface porosity, and bulk porosity therefore remains the rate-limiting factor that dominates permeability.

Section 18- Flow rates

To fully quantify the effect of the tungsten powder, the relationship between surface pore size and flux needs to be considered. Table 5 compares the percentage change of both pore size and flux of a selection of as-received and tungsten powder-coated samples. It can be seen that after coating, the surface is clearly being modified with the pore size being reduced by an average of 47 %. The reduction in pore size also affects gas flow through the substrate, with an average decrease in flux of 19 %. The relationship between pore size and flux does not show a strong correlation. Sample 11 exhibits the highest percentage reduction in pore size, with a value of 72 % and only a reduction of 24 % in flux, whereas sample 8 only reduced pore size by 45%, however still had a similar reduction in flux of 25 %. This shows that reducing pore size does not necessarily correlate with an increase in flux reduction.

Table 4 also shows that a significantly large reduction in pore size, up to 72 % does not significantly affect the H_2 flux through the substrate. A maximum reduction in flux of 28 % was observed, which shows that the surface pore size can be significantly reduced before permanence is dramatically affected.

A decrease of only 19 % is relatively small when considering the whole composite membrane and a large reduction in pore size of nearly 50 % will ultimately enable a thin membrane layer to be coated. This result strikes the important balance between reduction in pore size and minimising resistance to gas flow, which will help to meet the stringent USA DoE targets.

Table 5-Percentage differences of pore size and flux after PSS substrates were coated with tungsten powder.

Sample/Tungsten layer	As-received		W powder-coated		% Difference-Pore size	% Difference - Flux
	Pore size (µm)	Flux (ml/min)	Pore size (µm)	Flux (ml/min)		
3-1t	0.665	750.3	0.576	613.3	12.8	18.3
5-3t	1.06	771.9	0.409	554.2	61.4	28.2
8-3t	0.578	731.8	0.318	545.8	44.9	25.4
10-1t	0.877	769.2	0.538	682.1	38.7	11.3
11-3t	0.547	636.2	0.151	479.9	72.4	24.6
12-3t	0.714	600.4	0.349	557.5	51.1	7.2
Mean					46.9	19.2
Standard deviation					20.6	8.4

In terms of hydrogen transport, this finding also agrees with previous literature which also found that surface porosity could be reduced significantly before the permeance was affected [19].

Section 19- Stainless steel coating

The next stage of the process was to coat the samples with varying thicknesses of stainless steel to understand how pore-filling effects the production of a continuous defect-free layer. SEM secondary electron images were taken of both (1 and 3) tungsten layers at various thicknesses of stainless steel, (5, 10, 20, 30 µm) the results are shown in Figure 19 - Figure 22.

The images clearly show the progressive thickness of the sputtered stainless steel layer from 5 to 30 µm. As the SS layer becomes thicker, the underlying porous structure becomes less visible. The first image in Figure 19 has a 5 µm coating and 1 treatment of tungsten, it is clear that the underlying porous structure is still visible. The tungsten powder is not filling the PSS surface pores sufficiently enough with only one layer, the pores are still too deep for a thin 5 µm continuous layer. However, there are signs of greater tungsten coverage in the second image in Figure 19, where the sample has been treated with 3 layers of tungsten. It is clear that the increase in pore-filling has resulted in a more continuous layer of SS, with less visible larger pores and the majority of the smaller pores being coated successfully.

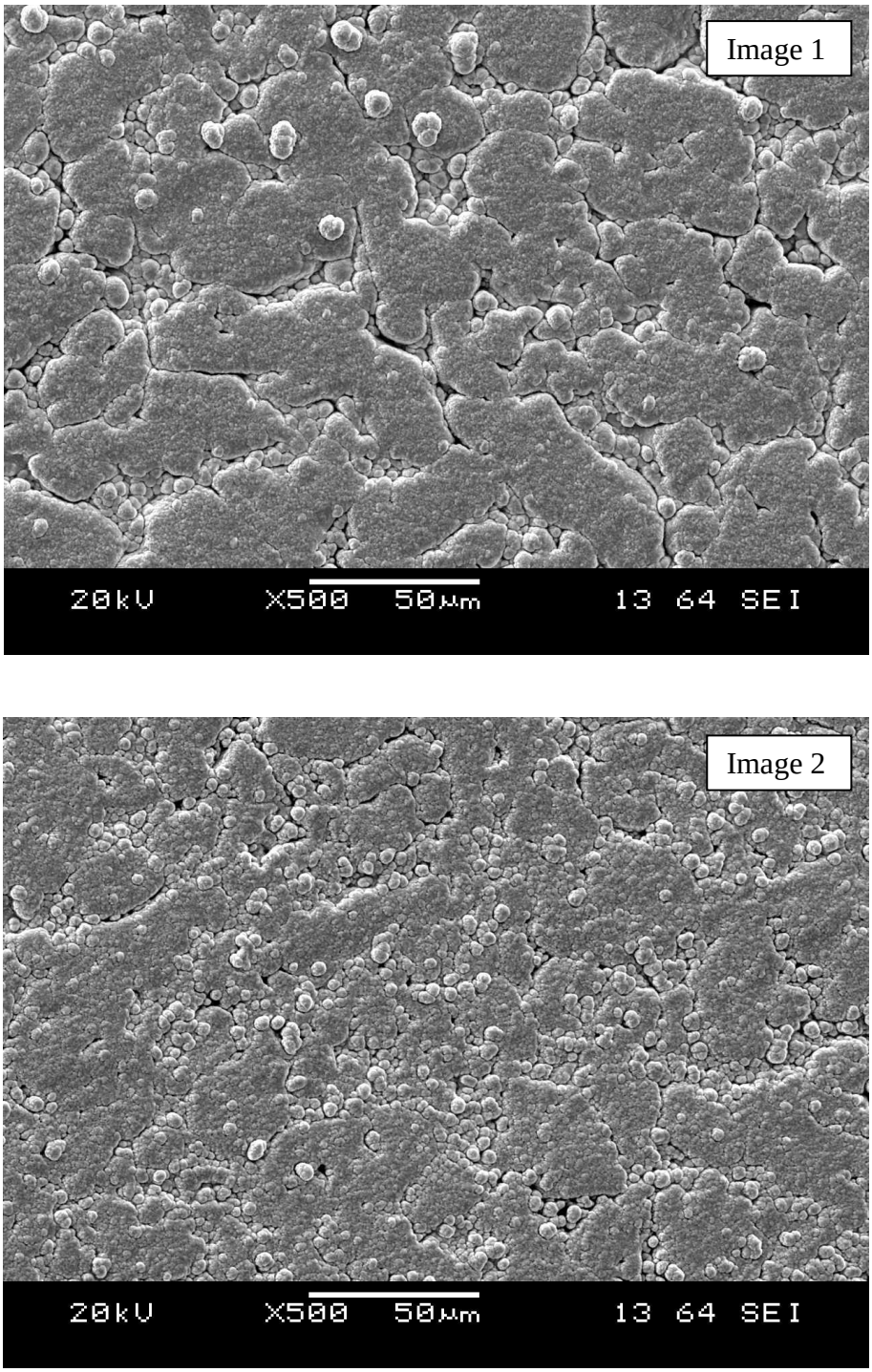

Figure 19- SEM secondary electron image showing 1 layer of tungsten powder+ 5 µm SS and 3 layers of tungsten powder +5 µm SS

As the coating thickness is increased to 10 µm, surface pores still remain clearly visible. Again there is a difference between the 1 and 3 layers of tungsten, however this time the 1 layer (Figure 20) seems to have a marginally more continuous layer with less visible cracks

and defects being seen. An explanation for this could be due to the unpredictable nature of the 3 layer coating. In Section 16, it was seen that increasing the amount of tungsten powder could caused clumping on the surface, which in turn creates a surface topography that inhibits the coating of a continuous layer.

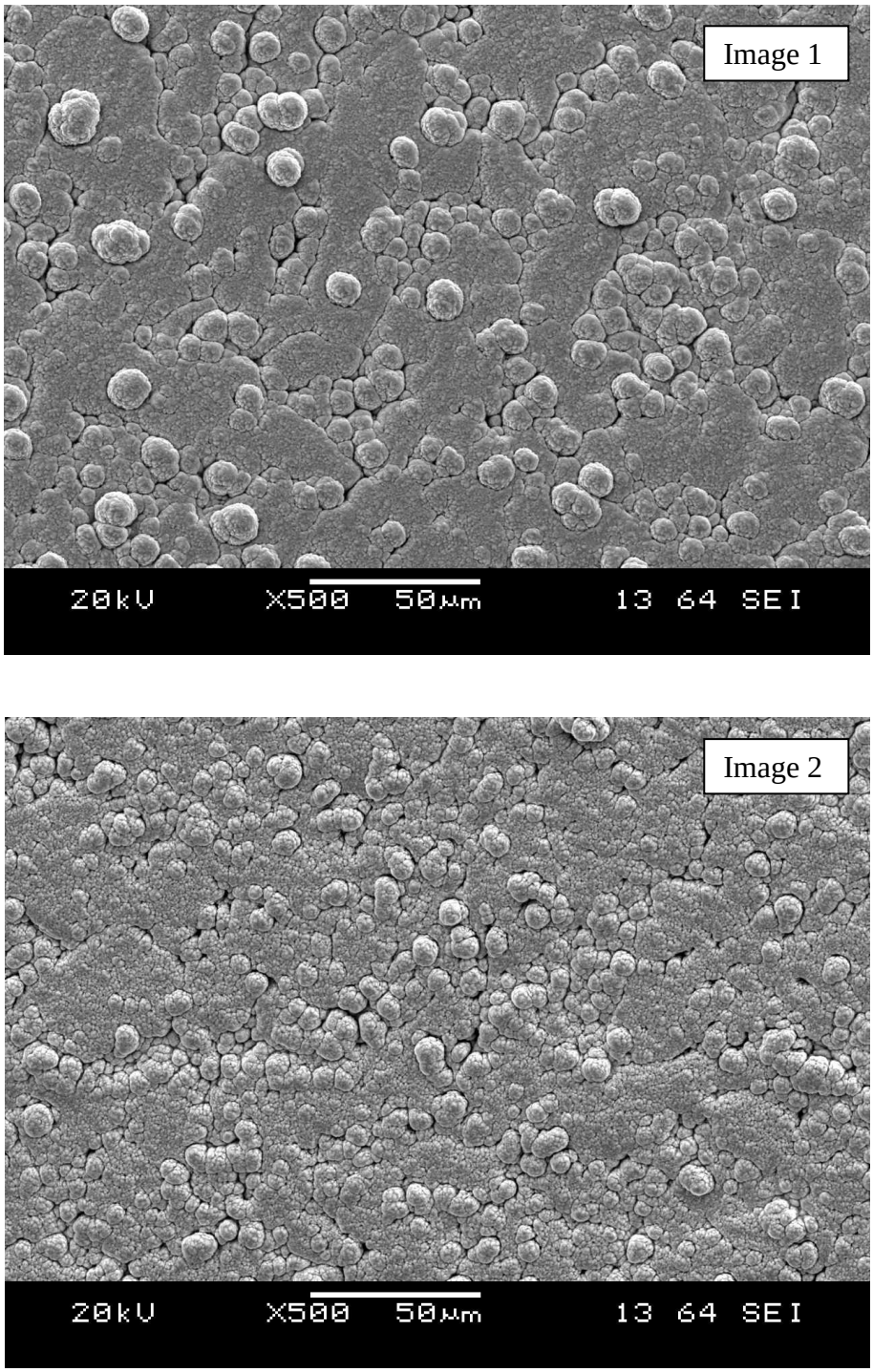

Figure 20- SEM secondary electron images- 1 layer of tungsten powder+10 µm SS and 3 layer of tungsten powder + 10 µm SS

The micrographs (Figure 21 and Figure 22) of the samples coated with 20 and 30 µm of SS show that the effectiveness of the SS layer is clearly dependant on the evenness of the tungsten intermediate layer. Both images in Figure 21 are coated with 3 layers of tungsten

powder yet the appearance of the stainless steel coverage is significantly different. Image 1 seems to have large cracks within the SS layer compared to image 2, which can only mean that the underlying tungsten layer is not consistent. When depositing 3 layers of tungsten there is a degree of variation between the amounts of tungsten being deposited onto the surface. This variation has resulted in mixed success when coating the stainless steel layer, as some samples have been more evenly coated than others. Some of the samples coated with 3 layers have suffered from powder clumping on the surface and have not been as successful as those with less clumping, highlighting the importance of having a uniform and consistent intermediate layer.

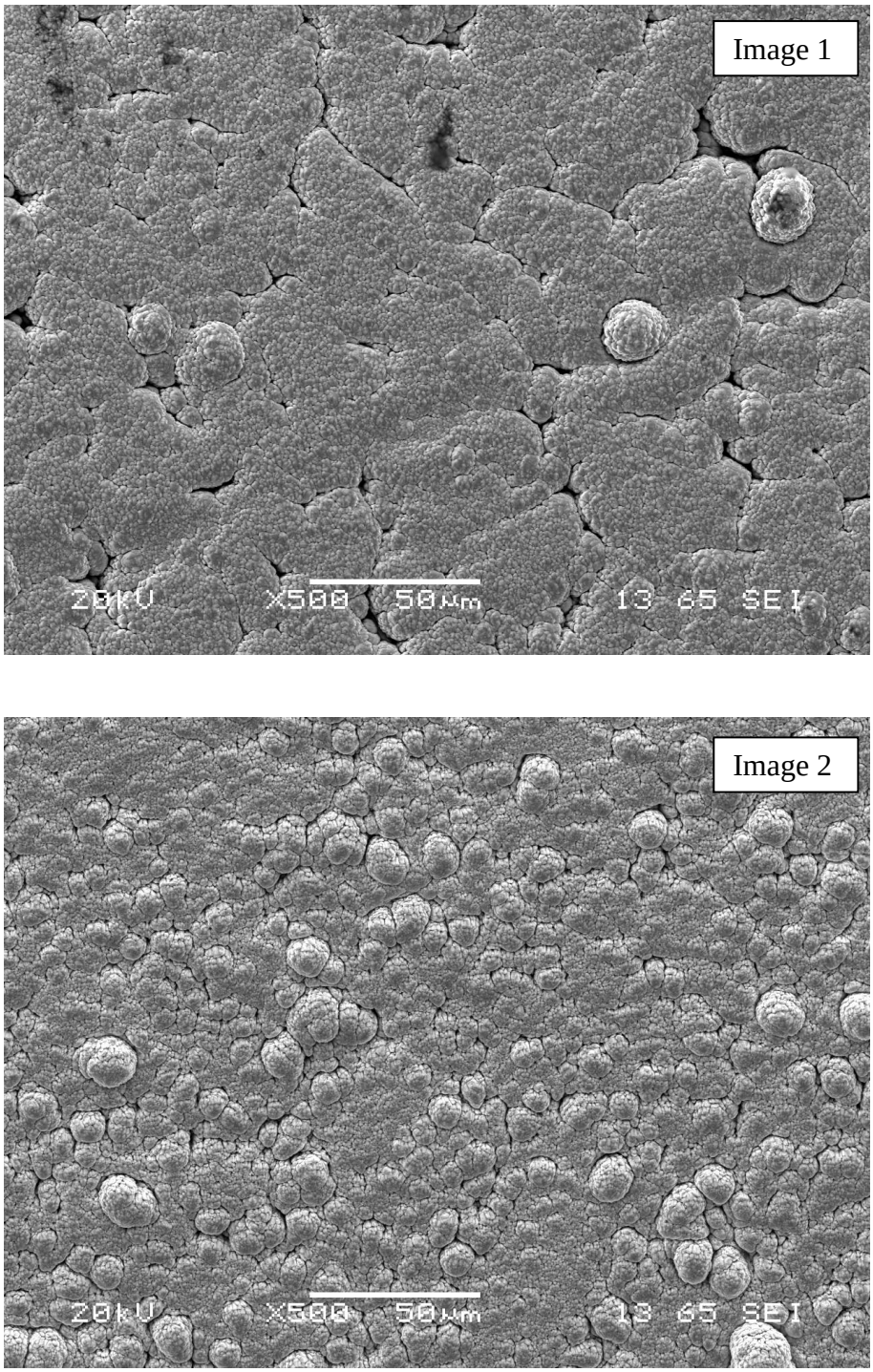

Figure 21- SEM secondary electron images showing 3 layers of W powder + 20 µm SS and 3 layers of W powder + 20 µm SS

Powder clumping is not a significant issue when only 1 layer of tungsten is being deposited, as the majority of the particles are pulled down into the pores by the applied vacuum. It is therefore easier to coat more consistent layers and without such a difference between

treatments. Image 1 and 2 in Figure 22 have both been treated with only one layer of tungsten and show to have similar SS coatings. Although it is easier to reproduce similar tungsten layers when coating only 1 layer, the insufficient pore-filling still results in defects, even after 30 µm coating of SS.

It is difficult to assess the performance of the tungsten layer by solely using SEM, so membranes permeability also needs to measured, in order to fully characterise the performance of the layer.

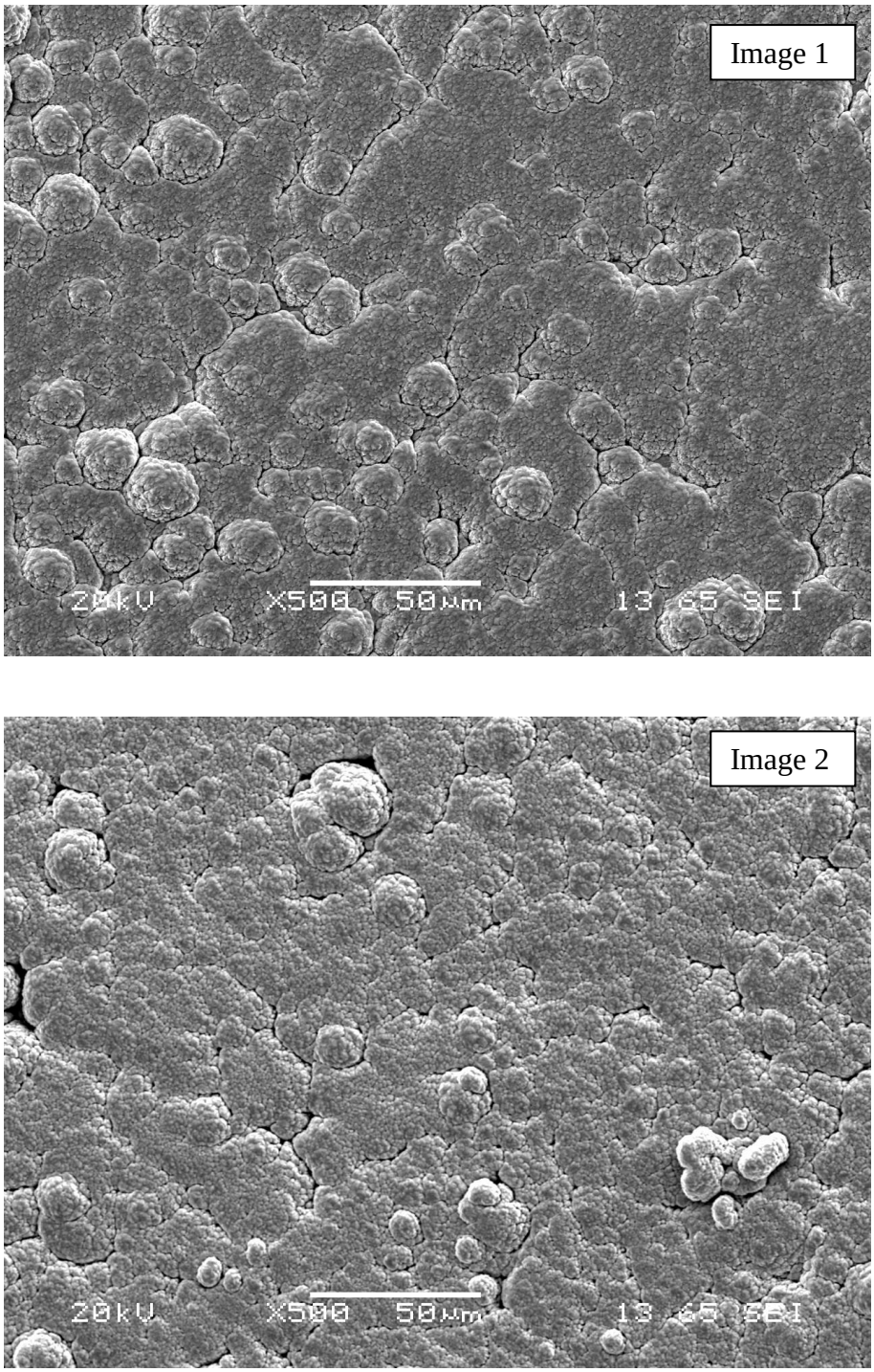

Figure 22- SEM secondary electron images showing 1 layer of W powder + 30 µm SS and 1 layer of W powder + 30 µm SS

Section 20- Stainless steel Permeability

In order to quantify the performance of the intermediate layer fully, it is necessary to analyse the measured hydrogen flux after the samples have been coated with stainless steel.

The permeability values determined before and after the samples were coated with either 5µm or 10 µm of SS are shown in Table 6 and Table 7, respectively. The difference in flux between the SS-coated samples and those only coated with tungsten, have been expressed as a percentage in flux reduction in order to characterise the performance. Table 6 shows that for the 3 tungsten layer there is 32 % reduction in flow, compared to only 14 % for the 1 layer sample. The amount of reduction in hydrogen flux through the composite membrane positively correlates with the performance of the SS layer. A greater reduction in flux, where hydrogen is blocked from passing through the membrane means that the SS layer is more continuous in nature with fewer defects. This also suggests that the intermediate tungsten layer is having the desired effect of reducing the surface pore size. This agrees with the observations seen in Figure 17 that showed the 3 layers filled more of the pores than the 1 layer.

Table 6- Percentage reduction in Hydrogen flux of 5 µm SS-coated PSS substrates with 3 layers of W powder

Sample:	Flux @ RT & 1 bar ΔP after W coating (ml/min)	Flux @ RT & 1 bar ΔP after SS coating (ml/min)	Percentage reduction in flux @ RT & 1 bar ΔP
Sample 15	586.2	503.0	14 %
Sample 4	540.3	369.2	32 %
Mean	563.3	436.1	23%
Standard deviation	32.5	94.6	12.7

The results for the samples coated with 5 µm of SS shown in Table 6 are not in agreement with those for the samples coated with 10 µm. The latter suggests that the 1 layer of tungsten is performing better than the 3 layers, having a larger percentage flux reduction of 62 %. An explanation for this, mentioned previously, is a result of the unpredictable nature of the depositing 3 layers of tungsten powder. It has been seen that the extent of the powder coating varied between samples, with some samples experiencing clumping on the surface. Clumping of the tungsten powder has a reverse effect on the topography of the surface and therefore acts in a similar way to a large pore, preventing the deposition of a continuous membrane layer. This suggests it is not necessarily the amount of tungsten pore-filling that has a significant effect, it is more dependent on how well and accurately the pores are filled.

Table 7- Percentage reduction in Hydrogen Flux of 10 µm SS coated PSS substrates with 1 layer of W powder.

Sample:	**W coating flux (mol.m^{-2}.s^{-1})**	**Flux after SS coating (mol.m^{-2}.s^{-1})**	**Percentage reduction in flux @ RT & 1 bar ΔP**
Sample 16	669.2	254.6	62 %
Sample 7	673.1	342.7	51 %
Mean	671.1	298.7	56.5%
Standard Deviation	2.8	62.3	7.8

The success of the two different intermediate layers is highlighted in Table 8 and Table 9. From the two tables it is clear to see that 3 tungsten layers have produced a wider variety of flux reduction when compared to the more consistent 1 layer. Sample 9 and 11 in Table 8, which have had identical tungsten powder pre-treatments, show a difference of 24 % in hydrogen flux reduction. Whereas, the samples displayed in Table 9, which have only 1 layer of tungsten powder, show a reduction in flux that is more similar, showing that the underlying tungsten surface is more consistent.

Table 8- Percentage flux reduction of PSS substrates coated with 20 µm of SS and with 3 layers of W powder.

Sample:	Flux @ RT & 1 bar ΔP after W coating (ml/min)	Flux @ RT & 1 bar ΔP after SS coating (ml/min)	Percentage reduction in flux @ RT & 1 bar ΔP
Sample 9	450.8	138.5	69 %
Sample 11	479.9	29.0	94 %
Sample 8	545.8	130.6	76 %
Sample 12	557.5	116.2	79 %
Mean	495.7	103.6	79.3%
Standard Deviation	65.4	50.6	10.0

Table 9- Percentage flux reduction of PSS substrates coated with 30 µm of SS and with 1 layer of W powder.

Sample:	Flux @ RT & 1 bar ΔP after W coating (ml/min)	Flux @ RT & 1 bar ΔP after SS coating (ml/min)	Percentage reduction in flux @ RT & 1 bar ΔP
Sample 2	681.7	84.5	88 %
Sample 3	613.3	101.5	82 %
Sample 1	622.2	6.9	99 %
Sample 10	682.1	128.0	81 %
Mean	649.8	80.2	87.5%
Standard Deviation	37.2	52.0	8.3

Section 21- Film adhesion, integrity and thickness

In order to produce layers of stainless steel at the correct thickness, test samples with SS coated onto glass slides were first produced, and it was found that film thickness deposition was linear with time. The samples were coated in 5 µm steps; this ensured that the layers built-up gradually, as opposed to one continuous layer which might cause undue stress on the bond between the PSS substrate and the SS layer.

The thickness was measured using a peel test, in which a strip of sticky tape was applied to the surface of the SS and then subsequently rapidly removed to reveal a well-defined edge. The average thickness over 5 different regions was 5.2 µm +/- 0.1 µm. (Figure 23). When removing the SS film, a small amount of residue from the tape was left behind on the glass slide, hence the small amount of surface roughness.

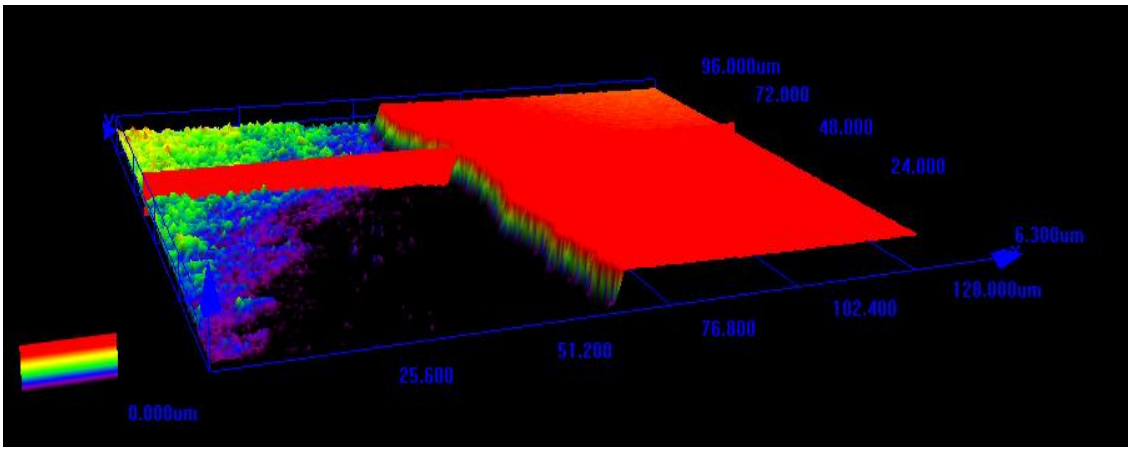

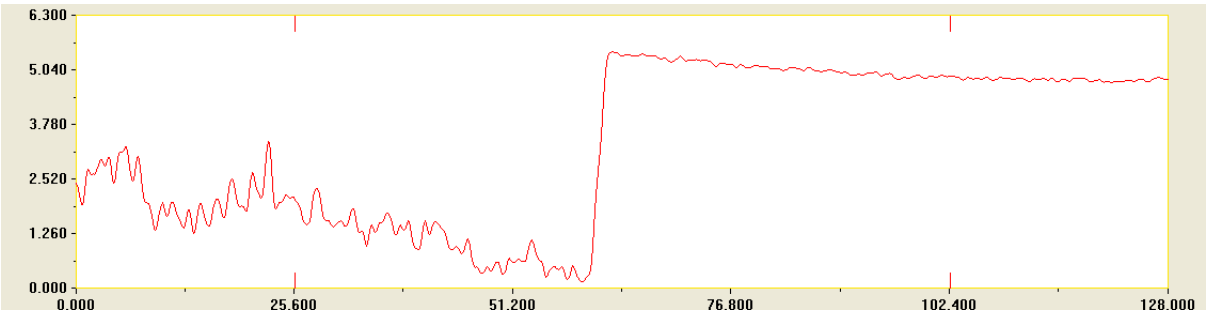

Figure 23 – Confocal laser image with line profile of a 2571 second SS coating on a PSS disc. Scale in (µm)

Section 22- Inter-diffusion layer

22.1 Introduction

In this section, the aim is to understand how a powdered tungsten intermediate layer affects interdiffusion between the PSS substrate and the Pd/PdCu layer. The intermediate tungsten layer was again, like the previous section, deposited onto PSS substrate samples in 1 and 3 layers. These composite samples were then coated with a 2.5 µm membrane of palladium or a palladium-copper alloy. The composite membranes were then heated under a helium atmosphere to 600°C. Longitudinal cross-sections were taken, and EDX analysis was used to track the migration of Fe to understand the extent, if any, of interdiffusion.

22.2 Alloy assessment and composition.

Room temperature X-ray diffraction patterns of a number of different Pd-Cu alloy compositions were analysed. Test compositions were crucial to be able to produce an alloy with a ratio as near to 60:40 Pd:Cu as possible. This desired composition is known to give the most desirable membrane properties such as high hydrogen permeability, sulphur tolerance and reduced cost [64]. It was not possible to simply follow the data in the literature as most sputtering systems work differently, so therefore 4 test coatings were carried out.

From the diffraction pattern (Figure 24), it is clear that none of the deposited films exhibit a single-phase solid solution composition. Therefore, in order to homogenise the Pd-Cu films they were loaded into an Anton Parr cell and heated in 50°C steps to 600°C in 1 bar helium. Figure 25 shows that after heat treatment the samples were fully homogenised.

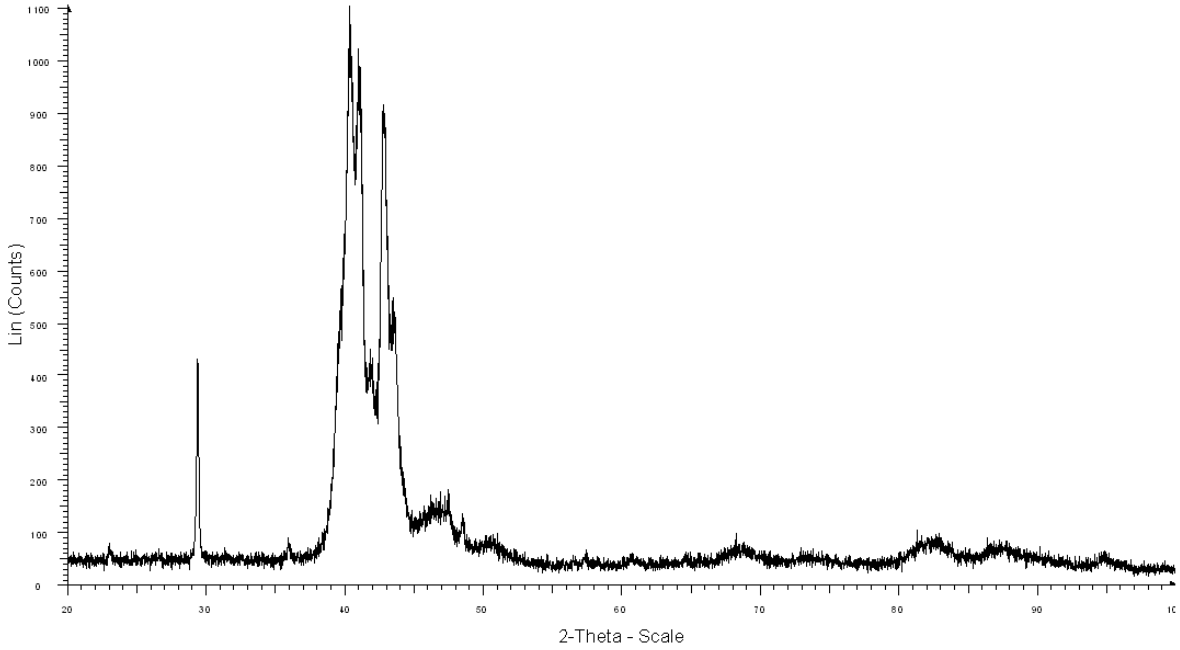

Figure 24- XRD trace from the alloy Pd-Cu 1 showing the non-homogeneous nature of the sample.

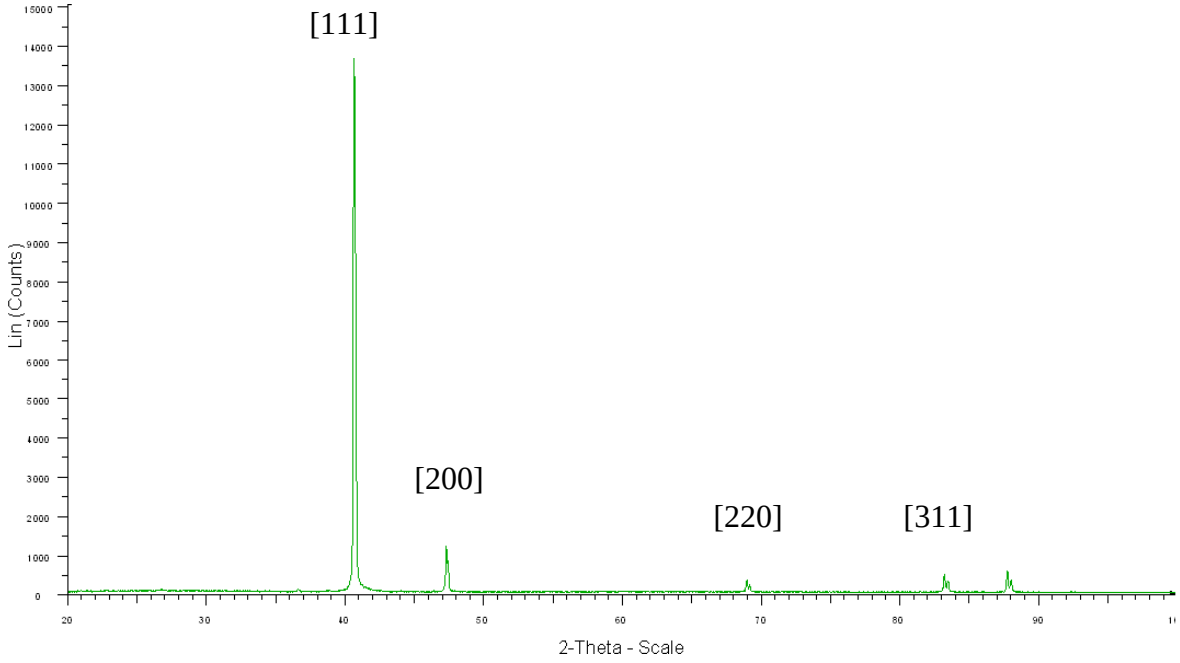

Figure 25- XRD trace showing homogenised Pd-Cu alloy after heating to 600ºC under a helium atmosphere.

Changing the compositions of the alloys was simply done by altering the current supplied to the Cu target, with the more amps applied to the target the greater the Cu percentage

deposited. The 4 currents used were: 0.25, 0.50, 0.75 and 1.0 A. The compositional data is given in Table 10.

Table 10- Compositions of Pd-Cu thin-films achieved using different Cu target voltages

Amps on Cu target	**d - Spacing (Å) ±0.0005**	**Lattice Parameter (a) (Å) ±0.0005**	**Calculated Composition (at. %) ± 0.07**
0.25	2.1924	3.692	18.2
0.50	2.1970	3.725	32.5
0.75	2.2159	3.733	47
1.0	2.2188	3.791	73

Alloy compositions were calculated by comparing the lattice parameters to existing literature values reported by Yang et al [37] using the linear equation;

$$y = (0.2705)\,x + 3.6343$$

Equation 22.1

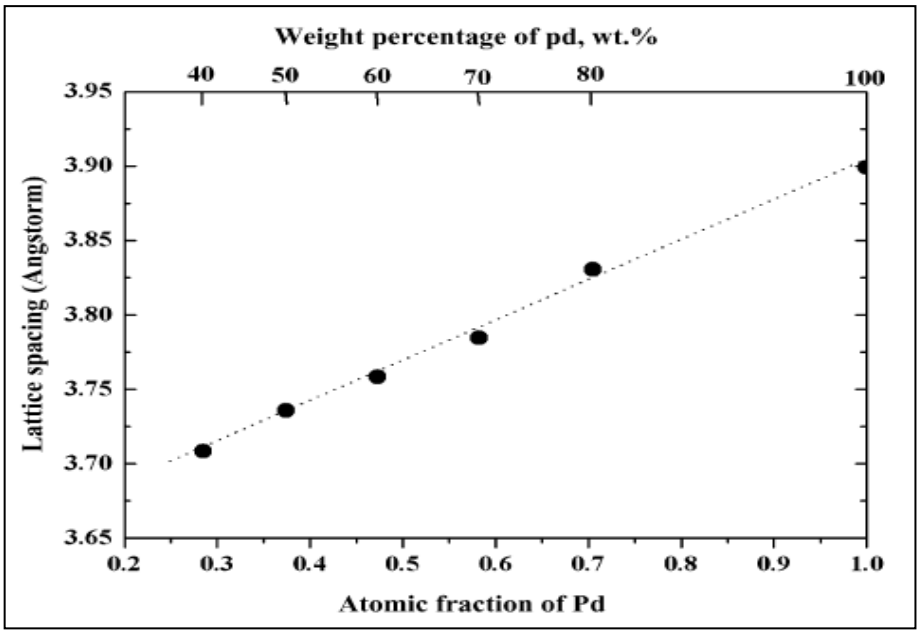

Figure 26- Correlation between lattice spacing and atomic fraction of Pd [37]

Where y is the measured lattice parameter and x is the atomic concentration of Pd. The lattice spacings were calculated using the d-spacings from the [111] peak. (This was because the [200], [220] and [311] peaks were not of sufficient intensity, to allow accurate values to be calculated).

The compositions are shown in Table 10 along with the d-spacing and lattice parameters. The graph in Figure 27 shows a linear relationship between Cu concentration and the number of amps supplied to the copper target.

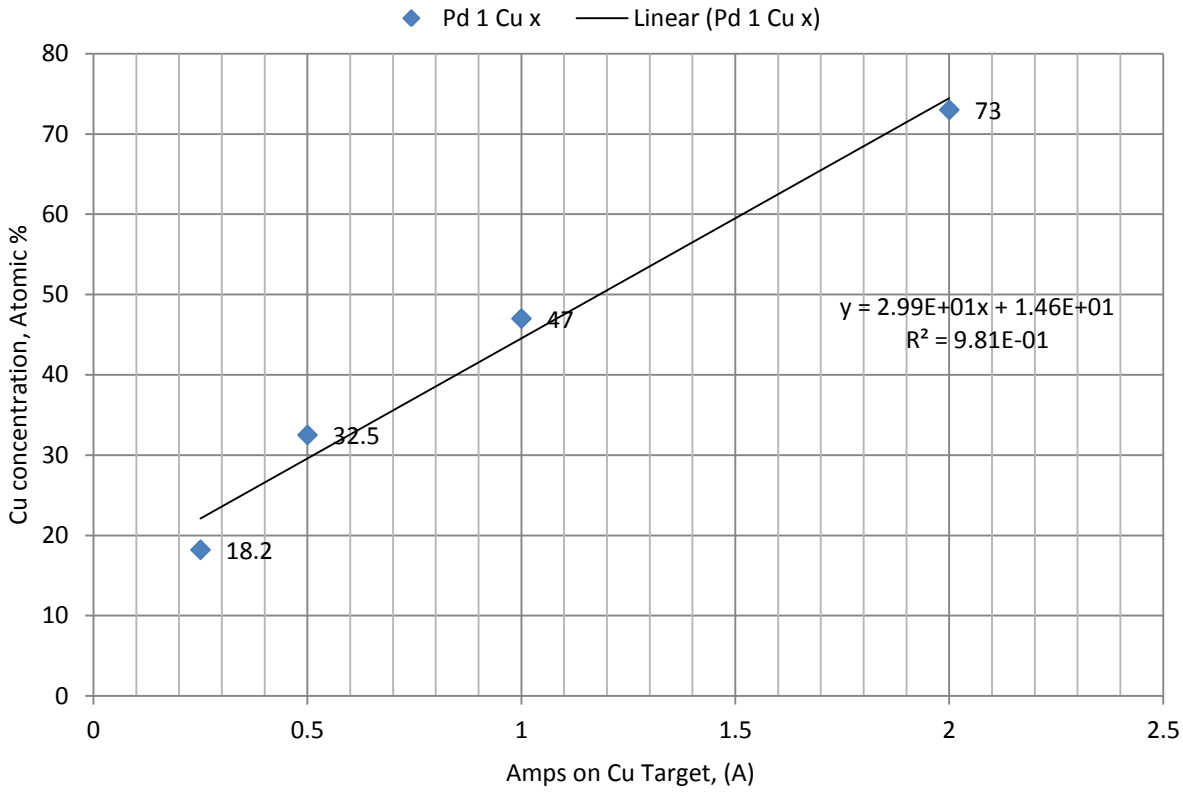

Figure 27- Cu target current versus the Cu atomic % composition of 4 different Pd-Cu thin-film alloys.

22.3 Interdiffusion

Whilst the primary function of the tungsten layer is to reduce the surface pore size of the PSS, its secondary function is to prevent the diffusion of iron from the substrate into the Pd/PdCu sputtered layer.

As before, 1 and 3 layers of tungsten were deposited onto the surfaces of the PSS substrate discs, which were then coated with either Pd or a Pd-Cu alloy. In addition to the powder tungsten layers, a PSS sample coated with a dense tungsten layer supplied by Teer Coatings Ltd was also coated with Pd-Cu. Each sample was subjected to 50°C step increases in temperature up to 600°C in 1 bar helium. Cross sections were cut off each sample and after setting in Bakelite were measured by SEM-EDX.

The ability of tungsten to prevent interdiffusion at temperatures up to 800°C as shown by Gryaznov et al [12], is supported in Figure 28. Tracking the amount of Fe across the membrane clearly shows that Fe migration is prevented by the dense tungsten layer.

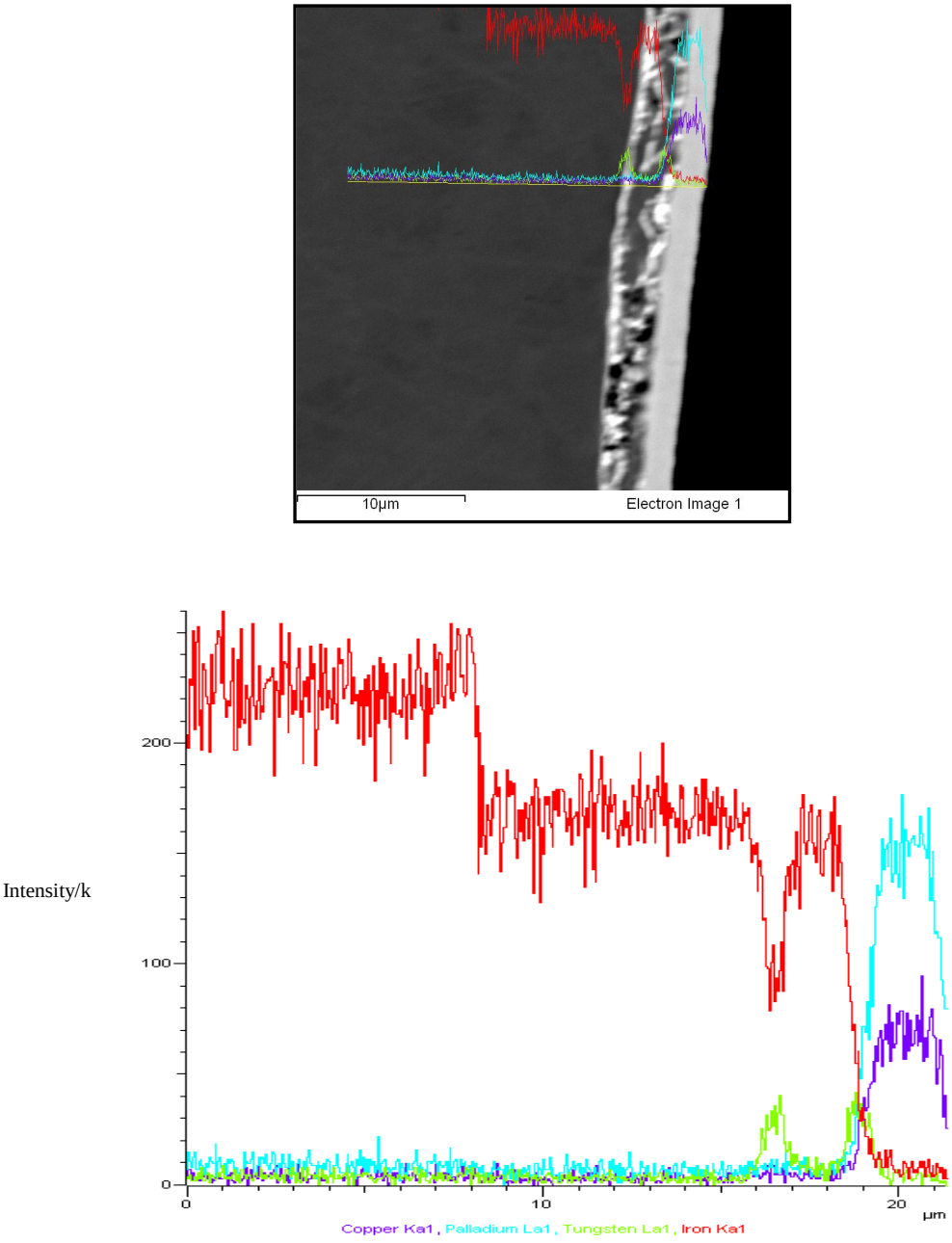

Figure 28- SEM backscattered image and EDX line scan of a PSS substrate coated with a dense sputtered W intermediate layer that has in turn been sputter coated with a thin-film Pd-Cu alloy.

The line scan in Figure 28 scans through the cross section of the dense tungsten composite sample. It shows that the presence of iron, represented by the red line, decreases intensity as soon as the tungsten layer is seen, represented by the green line. This finding shows that a thin layer of dense tungsten deposited onto the surface is successful at preventing interdiffusion. However, due to the very thin nature of the tungsten layer, areas in and around the surface pores will not be coated and therefore will be susceptible to iron diffusion.

Figure 29 shows two regions where EDX line scans examine the performance of the tungsten powder. Region 1 shows the surface of the pore, where the tungsten powder has not been deposited and Region 2 shows the cross section profile of an area where the tungsten powder particles have filled a surface pore.

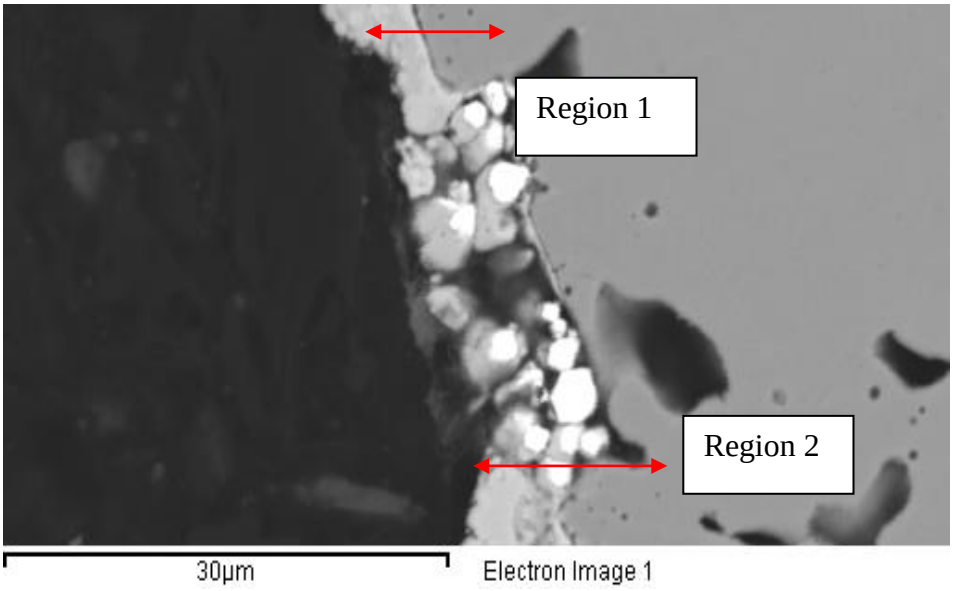

Figure 29- SEM image showing regions of EDX analysis from a sample coated with 1 layer of W powder and a sputtered PdCu alloy layer.

The elemental line scan (Figure 30) shows that in region 1 interdiffusion is taking place. The red line representing iron is clearly overlapping that of the palladium, meaning that iron has

diffused into the palladium layer. This is not unexpected as direct contact between stainless steel and palladium will lead to iron diffusion[48].

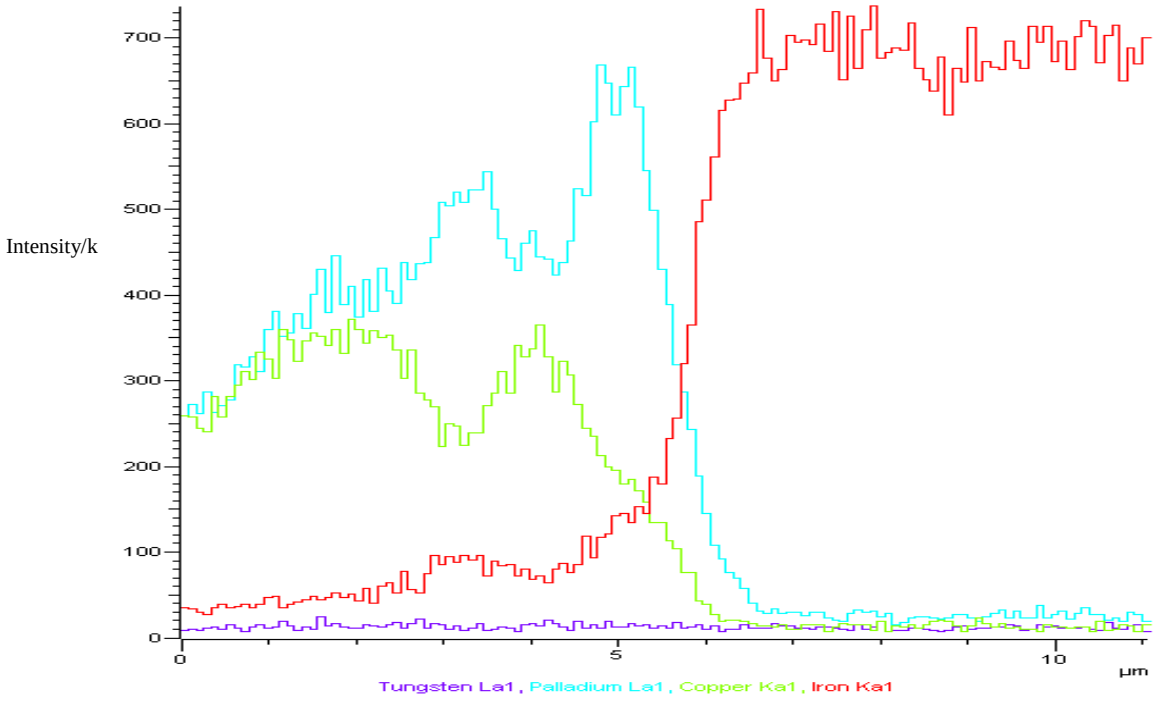

Figure 30- EDX line scan of region 1 taken from sample coated with 1 layer of W powder and a membrane layer of PdCu.

However, Figure 31 shows that the tungsten particles within the pore are working to limit interdiffusion by reducing direct contact between the steel and the palladium membrane layer. This result shows that tungsten powder deposited within the pores provides a significant interdiffusion barrier in which to prevent the diffusion of iron into the Pd / Pd-alloy.

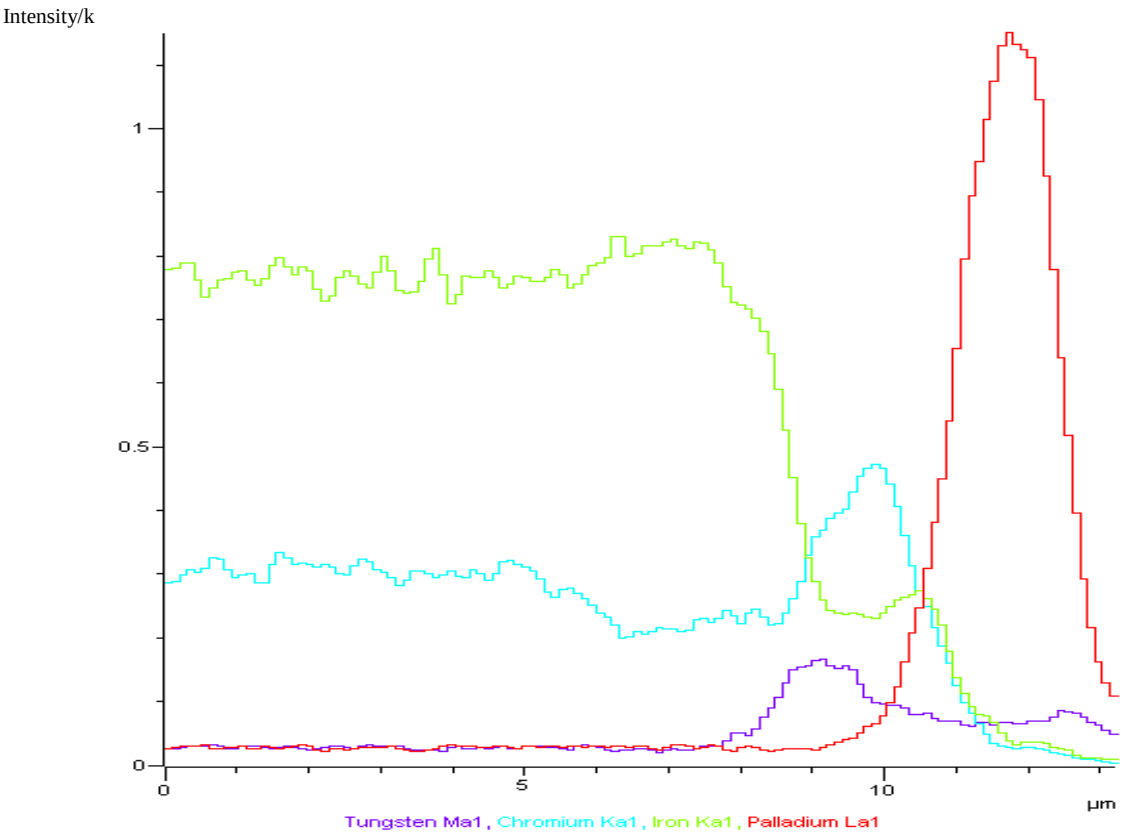

Figure 31- EDX line scan of region 2 taken from sample coated with 1 layer of W powder and a membrane layer of PdCu.

Filling only the surface pores of the substrate leaves areas of the PSS surface exposed to iron diffusion. Therefore, in order to both prevent interdiffusion within the pores and on the surface a combination of the thin dense layer seen in Figure 28 and the powder pore-filling will enable a much more extensive coverage and thus better performance against iron diffusion. Figure 32 simply shows how the two techniques would be used and which areas they cover.

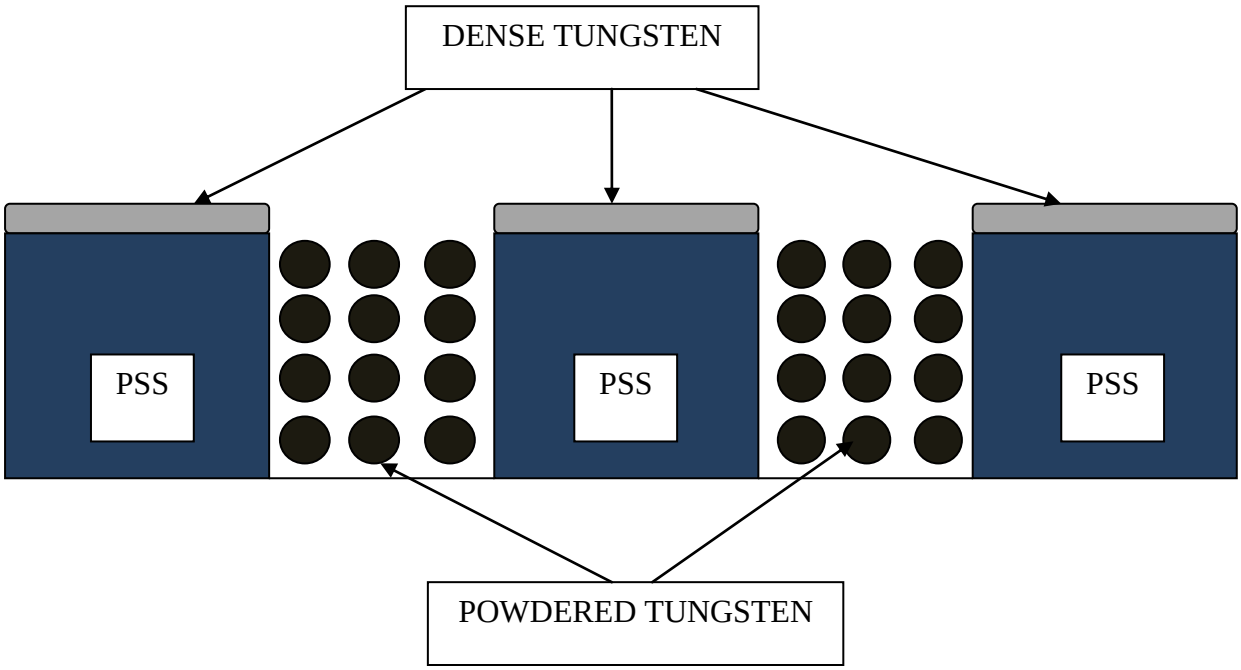

Figure 32- Schematic diagram showing the combination of a sputtered dense and a 1 µm powdered tungsten layer on a PSS substrate.

Chapter 5- Conclusions

Section 23- General Conclusions

Analysis of the modified surface and hydrogen permeation through the composite membrane has revealed that it is possible to reduce the overall pore depth and size without significantly affecting the permeance of the porous substrate. Although the amount of tungsten powder applied to the surface was not consistent, it was still possible to show that the quantity of powdered tungsten deposited onto the surface had no significant bearing on the hydrogen flux through the PSS disc. After 1 layer of tungsten there was an average decrease in hydrogen flux of 10% while there was only an 8% rise in resistance for 3 layers which does not show a significant increase.

Although large quantities of powder deposited onto the surface did not significantly affect the flow of hydrogen, the surface roughness associated with the powder distribution is a very important consideration, and has shown to directly affect the performance and thickness of the membrane layer. In order to produce a defect-free membrane layer, the surface of the PSS surface needs to be free from areas of powder clumping which cause an undulating surface profile. Ideally, surface roughness must be kept to a minimum, with the tungsten powder only occupying the pores and not residing on the surface.

The tungsten layers in this work varied from 1 or 3 layers. Depositing only 1 layer of tungsten was successful at reducing the surface pore depth by up to 50%, with the AR-PSS discs having an average pore depth of 8μm and the treated tungsten discs only having an average of 4μm. The deposition of tungsten, in conjunction with the applied vacuum enabled the powder

to primary be deposited within the surface pores and not on the surface; resulting in reduced surface roughness. Although successful at reducing pore depth and size, it failed to fully fill the pores to the extent whereby the surface was parallel with the tungsten in the pores. Half filling the surface pores still resulted in a fairly uneven surface topography, which therefore required a relatively thick SS coating of 20-30µm to be applied in order to obtain a continuous defect free membrane layer.

When examining the 3 layer coating an increased amount of tungsten powder within the pores and on the surface, was clearly visible. The increase in applied layers resulted in many more of the larger and deeper pores of the PSS being filled completely, with only a maximum pore depth of 2µm. Whilst this fulfils one of the major requirements and aims of the project, the success of the pore-filling was accompanied by clumping of excess powder on the surface, with powder peeks over 6µm tall. The clumping of the powder in and around the pores results in the surface topography having the reverse affect: protruding areas on the surface are effectively similar to having deep surface pores, as both prevent the deposition of a continuous membrane layer. Although both layers proved to be successful in reducing the pore depth and size, they both had drawbacks. In order to successfully produce a layer with all the right characteristics more time would need to be spent on refining the deposition technique, to insure the pores were filled to exact levels and overfilling was not encountered.

The importance of having an intermediate layer that fully fills the surface pores without overfilling was highlighted when coating stainless steel onto the modified PSS disc. Depositing SS onto the modified surface enabled performance characterisation of the tungsten layers in terms of producing a continuous defect-free layer. When the modified PSS samples were coated with SS layers of 5, 10, 20 and 30 µm, it was clear that the intermediate tungsten layer was having a significant effect on reducing the surface pore size. Sample 11 had the

highest percentage pore reduction of 72.4% and after 20µm of SS showed a 94% reduction in hydrogen flux. The success of the tungsten layer was determined by how well and accurately the pores were being filled, with successful filling resulting in a more continuous SS layer which had a higher percentage of flux reduction. The extent of the continuous SS layer was measured by its ability to prevent hydrogen flux and was directly dependant on how successful the tungsten powder was at reducing the pore size and depth. Greater and more accurate pore filling as shown in sample 11 resulted in a smoother surface profile, which in turn lead to a more defect free continuous SS layer which gave a 93% reduction in hydrogen flux.

23.1 Further work

Whilst it has been shown that a powdered tungsten intermediate layer is successful in not significantly inhibiting the flow of hydrogen, the way in which it is deposited is a factor that needs further research. In order to deposit an effective continuous defect-free layer, 3 main objectives need to be adhered to: reduce the transport resistance; minimise surface roughness; and limit the maximum surface pore size. This project has shown that a powdered tungsten intermediate layer does not affect the transport resistant; however refinement of the layer needs further consideration in order to fulfil the other two requirements.

The deposition technique needs to be further developed in order to deposit a tungsten layer that not only fills the surface pores but also does not overfill and clump. This could be achieved by refining the amount of tungsten powder used and the average particle size. A more stringent process whereby small increases of powder by weight could be used to understand the exact amount of tungsten powder needed to fill the pores without overfilling.

An agitator could possibly be used to vibrate the surface of the PSS disc to increase pore-filling. Agitating the surface combined with the vacuum already used might encourage the powder particles to fill the pores more evenly and not to reside on the surface.

Using a different solution to suspend the tungsten powder should be investigated. A liquid with a lower viscosity would suspend the particles more uniformly, thus aiding the deposition process by enabling more comprehensive powder coverage.

The observed discrepancies between the consistencies of the layers coated with the same amount of tungsten layers suggest that the technique used for deposition needs further consideration. In order to eliminate human error, a machine or mechanical device that deposits powder particles evenly across a surface could be used to coat the samples and this may increase the consistency of the deposited layers.

Combination of the powdered tungsten layer and the dense layer must also be further examined. Combining the two techniques is the next progression in order to fully understand the ability of tungsten to prevent diffusion of iron from the substrate into the membrane layer. Further work is needed to establish whether or not the combination of the two techniques, will be sufficient in preventing such iron migration.

Reference list

1. Nenoff, T.M., Spontak, R.J., and Aberg, C.M., , *Membranes for hydrogen purification: An important step toward a hydrogen based economy.* . MRS Bulletin 2006. **31**: p. 735.
2. Lu, G.Q., Costa, J.C., Duke, M., Giessler, S., Socolow, R., Williams, R.H., and Kreutz, T., , *Inorganic membranes for hydrogen production and purification: A critical review and perspective.* Journal of Colloid and Interface Science, 2007. **314**(2): p. 589-603.
3. Dolan, M.D., Dave, N. C., Ilyushechkin, A. Y., Morpeth, L. D., McLennan, K. G., *Composition and operation of hydrogen-selective amorphous alloy membranes.* Journal of Membrane Science, 2006. **285**(1-2): p. 30-55.
4. ***The hydrogen economy:*** *Opportunities, Costs, Barriers and R&D needs. Commitee on alternatives and strategies for future hydrogen production and use* N.r. council, Editor. 2005, National academy of engineering: Washington, DC.
5. Hagg, M.B., Quinn, R., *Polymeric facilitated transport membranes for hydrogen purification.* Mrs Bulletin, 2006. **31**(10): p. 750-755.
6. Cheng, X., Shi, Z., Glass, N., Zhang, L., Zhang, J., Song, D., Liu, Z.S., Wang, H., and Shen, J., , *A review of PEM hydrogen fuel cell contamination: Impacts, mechanisms and mitigation.* . Journal of Power Sources 2007 **165** p. 739. .
7. DoE., U.S., *Technical plan- Hydrogen production*. 2003. p. 17.
8. Tosti, S., Bettinali, L., Castelli, S., Sarto, F., Scaglione, S., Violante, V., *Sputtered, electroless, and rolled palladium-ceramic membranes.* Journal of Membrane Science, 2002. **196**(2): p. 241-249.
9. Lee, D.W., Lee, Y.G., Nam, S.E., Ihm, S.K., and Lee, K.H., , *Study on the variation of morphology and separation behavior of the stainless steel supported membranes at high temperature.* Journal of Membrane Science, 2003. **220**(1-2): p. 137-153.
10. Huang, Y., Dittmeyer, R., *Preparation of thin palladium membranes on a porous support with rough surface.* Journal of Membrane Science, 2007. **302**(1-2): p. 160-170.
11. Ma, Y.H., Akis, B.C., Ayturk, M.E., Guazzone, F., Engwall, E.E., and Mardilovich, I.P., , *Characterization of Intermetallic Diffusion Barrier and Alloy Formation for Pd/Cu and Pd/Ag Porous Stainless Steel Composite Membranes.* Industrial & Engineering Chemistry Research, 2004. **43**(12): p. 2936-2945.
12. Gryaznov, V.M., Serebryannikova, O. S., Serov, Y. M., Ermilova, M. M., Karavanov, A. N., Mischenko, A. P., Orekhova, N. V., *PREPARATION AND CATALYSIS OVER PALLADIUM COMPOSITE MEMBRANES.* Applied Catalysis a-General, 1993. **96**(1): p. 15-23.
13. Shirasaki, Y., Tsuneki, T., Ota, Y., Yasuda, I., Tachibana, S., Nakajima, H., Kobayashi, K., *Development of membrane reformer system for highly efficient hydrogen production from natural gas.* International Journal of Hydrogen Energy, 2009. **34**(10): p. 4482-4487.
14. Energy, U.S.D.o. *Hydrogen production*. www1.eere.energy.gov 2011.
15. Miller, G.Q., and Stocker, J., , *Selection of a hydrogen separation process* in *National Petrochemical and Refiners Association* 1989: San Francisco, CA, .
16. Ward, T.L., Dao, T, *Model of hydrogen permeation behaviour in palladium membranes.* Journal of Membrane Science, 1999. **153**: p. 211
17. Buxbuam, R.E., Marker, T.L., *Hydrogen transport through non-porous membranes of Pd coated Nb,Ta and V.* Journal of Membrane Science, 1993. **85**: p. 29.
18. Kamakoti, P., Sholl, D. S., *Towards first principles-based identification of ternary alloys for hydrogen purification membranes.* Journal of Membrane Science, 2006. **279**(1-2): p. 94-99.
19. Fletcher, S., *Thin film Palladium - Yttrium membranes for hydrogen separation* in *School of Metallurgy and Materials* 2009, UNIVERSITY OF BIRMINGHAM: Birmingham. p. 267.

20. Zeng, G., Goldbach, A., and Xu, H.Y., , *Impact of support mass flow resistance on low-temperature H2 permeation characteristics of a Pd95Ag5/Al2O3 composite membrane.* Journal of Membrane Science, 2009. **326**(2): p. 681-687.
21. Checchetto, R., Bazzanella, N., Patton, B., Miotello, A., *Palladium membranes prepared by r.f. magnetron sputtering for hydrogen purification.* Surface and Coatings Technology, 2004. **177-178**: p. 73-79.
22. McCool, B., Xomeritakis, G., Lin, Y. S., *Composition control and hydrogen permeation characteristics of sputter deposited palladium-silver membranes.* Journal of Membrane Science, 1999. **161**(1-2): p. 67-76.
23. Xomeritakis, G.a.L., Y. S., *Fabrication of thin metallic membranes by MOCVD and sputtering.* Journal of Membrane Science, 1997. **133**(2): p. 217-230.
24. Jayaraman, V., Lin, Y. S., Pakala, M., Lin, R. Y., *Fabrication of ultrathin metallic membranes on ceramic supports by sputter deposition.* Journal of Membrane Science, 1995. **99**(1): p. 89-100.
25. Zhao, H.B., Xiong, G. X., Baron, G. V., *Preparation and characterization of palladium-based composite membranes by electroless plating and magnetron sputtering.* Catalysis Today, 2000. **56**(1-3): p. 89-96.
26. Roa, F., Way, J. D., McCormick, R. L., Paglieri, S. N., *Preparation and characterization of Pd-Cu composite membranes for hydrogen separation.* Chemical Engineering Journal, 2003. **93**(1): p. 11-22.
27. Ye, J., Dan, G., and Yuan, Q., , *The permeation of ultrathin Pd membranes.* . Key Eng. Mater., , 1991. **60-61**: p. 437.
28. Ma, Y.H., Mardilovich, I.P., and Mardilovich, P.P., , *Effects of porosity and pore size distribution of the porous stainless steel on the thickness and hydrogen flux of palladium membranes* J. Amer. Chem. Soc, , 2001. **46**(2).
29. Graham, T., *Absorption and separation of gases by colloid septa.* . Phil. Trans. Roy. Soc, , 1866 **156(399)** p. 426
30. Wise, M.L.H., Farr, J. P. G., Harris, I. R., *X-ray studies of the [alpha]/[beta] miscibility gaps of some palladium solid solution-hydrogen systems.* Journal of the Less Common Metals, 1975. **41**(1): p. 115-127.
31. Jewell, L.L., Davies, B.H., , *Review of absorption and adsorption in the hydrogen-palladium system.* Applied Catalysis A: General, 2006. **310**: p. 1-15.
32. Keuler, J.N., Lorenzen, L., *Developing a heating procedure to optimise hydrogen permeance through Pd-Ag membranes of thickness less than 2.2 [mu]m.* Journal of Membrane Science, 2002. **195**(2): p. 203-213.
33. Meng, G.Y., Huang, L., Pan, M., Chen, C. S., Peng, D. K., *Preparation and characterization of Pd and Pd-Ni alloy membranes on porous substrates by MOCVD with mixed metal [beta]-diketone precursors.* Materials Research Bulletin, 1997. **32**(4): p. 385-395.
34. Thoen, P.M., F. Roa, and J.D. Way, *High flux palladium-copper composite membranes for hydrogen separations.* Desalination, 2006. **193**(1-3): p. 224-229.
35. Roa, F., Way, J.D., , *The effect of air exposure on Pd-Cu composite membranes.* . Applied Surface Science, 2005. **240**: p. 85.
36. Gao, H.Y., Lin, J. Y. S., Li, Y. D., Zhang, B. Q., *Electroless plating synthesis, characterization and permeation properties of Pd-Cu membranes supported on ZrO2 modified porous stainless steel.* Journal of Membrane Science, 2005. **265**(1-2): p. 142-152.
37. Yang, J.Y., Nishimura, C., Komaki, M., *Preparation and characterization of Pd-Cu/V-15Ni composite membrane for hydrogen permeation.* Journal of Alloys and Compounds, 2007. **431**(1-2): p. 180-184.
38. Zhang, Y., Ozaki, T., Komaki, A., Nishimura, C., *Hydrogen permeation of Pd-Ag alloy coated V-15Ni composite membrane: effects of overlayer composition.* Journal of Membrane Science, 2003. **224**(1-2): p. 81-91.

39. Ryi, S.K.P., J. S. Kim, S. H. Cho, S. H. Kim, D. W. Um, K. Y., *Characterization of Pd-Cu-Ni ternary alloy membrane prepared by magnetron sputtering and Cu-reflow on porous nickel support for hydrogen separation.* Separation and Purification Technology, 2006. **50**(1): p. 82-91.
40. Klette, H., Bredesen, R., *Sputtering of very thin palladium-alloy hydrogen separation membranes.* Membrane Technology, 2005. **2005**(5): p. 7-9.
41. Keuler, J.N., Lorenzen, L., Sanderson, R. N., Linkov, V., *Optimizing palladium conversion in electroless palladium plating of alumina membranes.* Plating and Surface Finishing, 1997. **84**(8): p. 34-40.
42. Sun, G.B., Hidajat, K., Kawi, S., *Ultra thin Pd membrane on alpha-Al2O3 hollow fiber by electroless plating: High permeance and selectivity.* Journal of Membrane Science, 2006. **284**(1-2): p. 110-119.
43. Huang, T.C., Wei, M.C., and Chen, H.I., , *Preparation of hydrogen-permselective palladium-silver alloy composite membranes by electroless co-deposition.* Separation and Purification Technology, 2003. **32**(1-3): p. 239-245.
44. Hou, K., Hughes, R., *Preparation of thin and highly stable Pd/Ag composite membranes and simulative analysis of transfer resistance for hydrogen separation.* Journal of Membrane Science, 2003. **214**(1): p. 43-55.
45. Wu, L.Q., Xu, N. P., Shi, J., *Preparation of a palladium composite membrane by an improved electroless plating technique.* Industrial & Engineering Chemistry Research, 2000. **39**(2): p. 342-348.
46. Uemiya, S., Kude, Y., Sugino, K., Sato, N., Matsuda, T., Kikuchi, E., *A PALLADIUM POROUS-GLASS COMPOSITE MEMBRANE FOR HYDROGEN SEPARATION.* Chemistry Letters, 1988(10): p. 1687-1690.
47. Ryi, S.K., Park, J.S., Choi, S.H., Cho, S.H., and Kim, S.H., , *Fabrication and characterization of metal porous membrane made of Ni powder for hydrogen separation.* Separation and Purification Technology, 2006. **47**(3): p. 148-155.
48. Mardilovich, P.P., She, Y. Ma, Y. H., Rei, M. H., *Defect-free palladium membranes on porous stainless-steel support.* Aiche Journal, 1998. **44**(2): p. 310-322.
49. Uemiya, S., Matsuda, T., Kikuchi, E., *HYDROGEN PERMEABLE PALLADIUM SILVER ALLOY MEMBRANE SUPPORTED ON POROUS CERAMICS.* Journal of Membrane Science, 1991. **56**(3): p. 315-325.
50. Bryden, K.J., Ying, J. Y., *Nanostructured palladium-iron membranes for hydrogen separation and membrane hydrogenation reactions.* Journal of Membrane Science, 2002. **203**(1-2): p. 29-42.
51. Burggraaf, A.J., *Chapter 9 Transport and separation properties of membranes with gases and vapours*, in *Membrane Science and Technology*, A.J. Burggraaf and L. Cot, Editors. 1996, Elsevier. p. 331-433.
52. Gabitto, J., Tsouris, C., *Hydrogen transport in composite inorganic membranes.* Journal of Membrane Science, 2008. **312**(1-2): p. 132-142.
53. Shu, J., Adnot, A., Grandjean, B. P. A., Kaliaguine, S., *Structurally stable composite Pd-Ag alloy membranes: Introduction of a diffusion barrier.* Thin Solid Films, 1996. **286**(1-2): p. 72-79.
54. Yepes, D., Cornaglia, L. M., Irusta, S., Lombardo, E. A., *Different oxides used as diffusion barriers in composite hydrogen permeable membranes.* Journal of Membrane Science, 2006. **274**(1-2): p. 92-101.
55. Bosko, M.L., et al., *NaA zeolite as an effective diffusion barrier in composite Pd/PSS membranes.* Journal of Membrane Science, 2009. **331**(1-2): p. 57-65.
56. Tong, J., Shirai, R., Kashima, Y., and Matsumura, Y., , *Preparation of a pinhole-free Pd-Ag membrane on a porous metal support for pure hydrogen separation.* Journal of Membrane Science, 2005. **260**(1-2): p. 84-89.

57. Nam, S.E., Lee, S.H., and Lee, K.H., , *Preparation of a palladium alloy composite membrane supported in a porous stainless steel by vacuum electrodeposition.* Journal of Membrane Science, 1999. **153**(2): p. 163-173.
58. Ma, Y.H.A., B. Ceylan Ayturk, M. Engin Guazzone, Federico Engwall, Erik E. Mardilovich, Ivan P., *Characterization of Intermetallic Diffusion Barrier and Alloy Formation for Pd/Cu and Pd/Ag Porous Stainless Steel Composite Membranes.* Industrial & Engineering Chemistry Research, 2003. **43**(12): p. 2936-2945.
59. Li, A., Grace, J.R., and Lim, C.J., , *Preparation of thin Pd-based composite membrane on planar metallic substrate: Part I: Pre-treatment of porous stainless steel substrate.* Journal of Membrane Science, 2007. **298**(1-2): p. 175-181.
60. Shu, J., Grandjean, B. P. A., Van Neste, A., Kaliaguine, S. , *Catalytic palladium-based membrane reactors: A review.* The canadian Journal of Chemical Engineering, 1991. **69**(5): p. 1036-1060.
61. Mottcorp. *Porous Metal Design Guidebook* 2010.
62. Qiao, A.L., Zhang, K., Tian, Y., Xie, L. L., Luo, H. J., Lin, Y. S., Li, Y. D., *Hydrogen separation through palladium-copper membranes on porous stainless steel with sol-gel derived ceria as diffusion barrier.* Fuel. **89**(6): p. 1274-1279.
63. Mardilovich, I.P., Engwall, E., Ma, Y. H., *Dependence of hydrogen flux on the pore size and plating surface topology of asymmetric Pd-porous stainless steel membranes.* Desalination, 2002. **144**(1-3): p. 85-89.
64. Paglieri, S.N.a.W., J.D., , *Innovations in Palladium Membrane Research. Separation and Purification Methods* 2002. **31 (1)**: p. 149.